

AD-A189 545

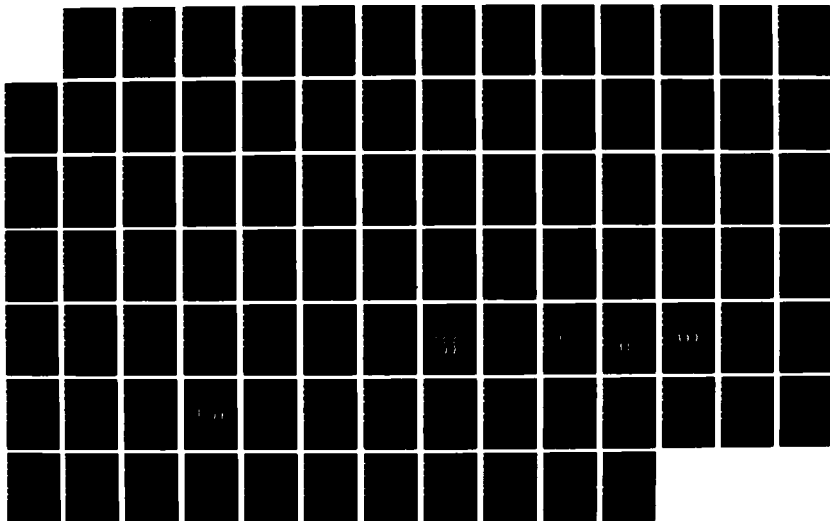
VISCOELASTIC BEHAVIOR OF A POLYETHERETHERKETONE (PEEK)
COMPOSITE(U) AIR FORCE INST OF TECH WRIGHT-PATTERSON
AFB OH SCHOOL OF ENGINEERING R P LOCKWOOD DEC 87
AFIT/GAE/AA/87D-10

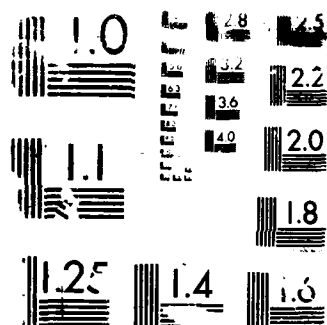
171

UNCLASSIFIED

F/G 11/4

NL

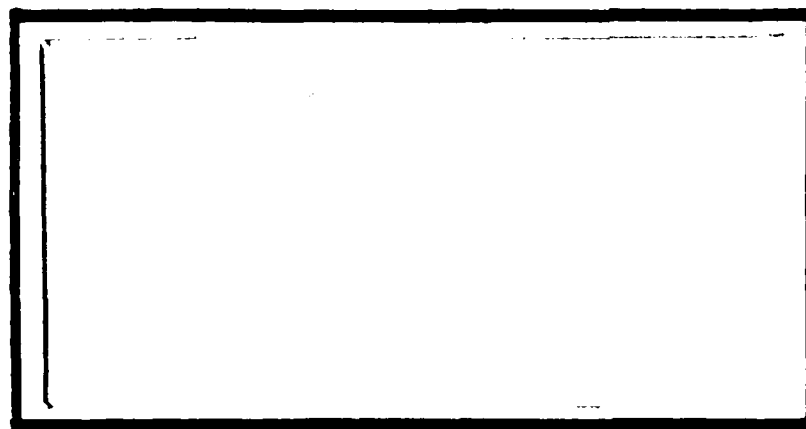




RESOLUTION TEST CHART

DTIC FILE COPY

AD-A189 545



DTIC
ELECTE
MAR 03 1988
S
H

DEPARTMENT OF THE AIR FORCE
AIR UNIVERSITY
AIR FORCE INSTITUTE OF TECHNOLOGY

Wright-Patterson Air Force Base, Ohio

DISTRIBUTION STATEMENT A

Approved for public release;
Distribution Unlimited

88 3 01 127

AFIT/GAE/AA/87D-10

VISCOELASTIC BEHAVIOR OF A
POLYETHERETHERKETONE (PEEK) COMPOSITE
THESIS

Richard P. Lockwood
Captain, USAF

AFIT/GAE/AA/87D-10

DTIC
ELECTE
MAR 03 1988
S H D

Approved for public release; distribution unlimited

AFIT/GAE/AA/87D-10

VISCOELASTIC BEHAVIOR OF A POLYETHERETHERKETONE
(PEEK) COMPOSITE

THESIS

Presented to the Faculty of the School of Engineering
of the Air Force Institute of Technology

Air University

In Partial Fulfillment of the
Requirements for the Degree of
Master of Science in Aeronautical Engineering

Richard P. Lockwood, B.S.

Captain, USAF

December 1987

Approved for public release; distribution unlimited

Preface

PEEK will fly in an F-18 Hornet this year. Is PEEK really that familiar now? The answer is yes and no. This research bridged the gap between the more commonly understood mechanical properties of the PEEK matrix and graphite fiber composite called APC-2 and the less well understood viscoelastic characteristics that it exhibits.

The flexure model developed here is a simple one, with viscoelastic parameters substituted for elastic material constants under assumed quasi-static conditions. Although the results are encouraging, my test technique can be improved, and these recommendations are respectfully passed on to the Materials Laboratory.

Without the sponsorship of the Non-Metallics Division, Structural Materials Branch, this study wouldn't have been possible. I am indebted to my sponsor, Dr. Charles Lee, and to his colleagues. I would like to single out the support of Mr. Ken Lindsay, Mr. Bill Ragland, and Ms. Margie Hudock.

Without the help of the faculty at AFIT, I would have misunderstood the importance of careful analysis. Special thanks to my advisor, Major Paul Copp, for the concern that he showed throughout this year.

Finally, this research would have been joyless had it not been for Paige, my wife. You kept the big picture near me at all times.

Richard P. Lockwood



Session For

GRA&I

TAB

ounded

Attention

tribution/

Availability Code

Avail and/or

Dist

Special

A-1

Table of Contents

	Page
Preface	ii
List of Figures	iv
List of Tables	vi
Abstract	vii
I. Introduction	1
II. Theory	7
III. Experimental Procedure	23
Materials	23
Test Equipment	27
Experimental Method	34
IV. Results	38
Transverse (90°) Behavior	43
Longitudinal (0°) Behavior	48
Master Curves	52
Shear Deformation	61
Comparison to Rule of Mixtures Approach	64
Shear Coupling Observations	69
V. Conclusion	71
Summary of Results	71
Conclusions	73
Recommendations	75
Bibliography	78
Vita	81

List of Figures

Figure	Page
1. Three Point Flexure Geometry	10
2. Functional Relationship of Dynastat Components	28
3. Thermal Stability of the Dynastat Chamber for 3 Steps	31
4. Static Flexural Response of a 90° Unidirectional APC-2 Specimen	39
5. Static Flexural Response of a PEEK Beam	41
6. Temperature Dependency of the Complex Flexural Moduli of APC-2, 90° Specimen, 1 rad/sec	42
7. Temperature Dependency of the Complex Flexural Moduli of APC-2, 90° Specimen, 10 rad/sec	44
8. Temperature Dependency of the Complex Flexural Moduli of APC-2, 90° Specimen, 100 rad/sec	45
9. Effect of Reduction Technique on 90° Specimen Shift Factors	47
10. Temperature Dependency of the Complex Flexural Moduli of APC-2, 0° Specimen	49
11. Effect of Reduction Technique on 0° Specimen Shift Factors	51
12. Master Curves of 90° Beam From "Super" Shifts of Storage Modulus	53
13. Master Curves of 90° Beam From Hand Shifts of Storage Modulus	55
14. Master Curves of 90° Beam From "Super" Shifts of Loss Modulus	56
15. Master Curves of 90° Beam From Hand Shifts of Loss Modulus	57

	Page
16. Master Curves of 0° Beam From "Super" Shifts of Storage Modulus	59
17. Master Curves of 0° Beam From Hand Shifts of Storage Modulus	60
18. Master Curves of 0° Beam From "Super" Shifts of Loss Modulus	62
19. Master Curves of 0° Beam From Hand Shifts of Loss Modulus	63
20. Temperature Dependency of the Complex Flexural Moduli of PEEK	66

List of Tables

Table	Page
1. Typical Mechanical Properties of APC-2 at 25°C	23
2. APC-2 Morphology	24
3. Comparison of the Experimental Complex Flexural Modulus With Shear Deformation Theory	64
4. Comparison Between Experimental Flexural Moduli And Values Predicted from the Rule of Mixtures	67

Abstract

The thermoplastic polyetheretherketone (PEEK) is being considered for structural applications in the Advanced Tactical Fighter. Previous efforts characterizing PEEK mechanical properties are reviewed. A study developing the viscoelastic frequency-temperature response to three point flexure of neat resin and PEEK/graphite fiber composites is detailed. The behavior of unidirectional laminates is compared to predictions from elastic plate theory, which also combines micro- and macromechanical approaches to predict transverse and longitudinal complex moduli. The experimental frequency-temperature shift factors, obtained under low strain in a Dynastat dynamic viscoelastic analyzer, are compared to shift factors predicted from the Williams-Landel-Ferry equation. Determining composite behavior from knowledge of matrix and fiber behavior is still applicable. The capability of the Dynastat to perform viscoelastic characterizations of stiff, unidirectional composites, based on comparisons of the various shift factors, is reduced due to the presence of the reinforcing fibers. Recommendations for future test and evaluations, including increasing the dynamic signal-to-noise ratio, are described. (The end)

VISCOELASTIC BEHAVIOR OF A POLYETHERETHERKETONE (PEEK) COMPOSITE

I. Introduction

Advances in aerospace vehicle performance often result from the improvements in the mechanical characteristics of the new materials in the vehicle. The design process requires material parameters in the stress analysis and in the study of failure mechanisms. This research characterizes the viscoelastic behavior of a thermoplastic and graphite fiber composite. The applicability of the three-point flexure to this characterization is considered, along with the effects of viscoelasticity on assumptions made in the development of an analysis of composite flexure.

The recent development of polyetheretherketone (PEEK), and its consideration for aerospace structural applications, results from the improved strength, toughness, stiffness, ease of producibility, resistance to solvents, and, of course, the light weight exhibited by graphite reinforced composites of the polymer. Some of the mechanical properties already known about this material are described below. Because PEEK is a polyaromatic resin, its continuous fiber reinforced composites have become known as aromatic polymer composites (APC).

Several different teams of researchers have examined PEEK and APC properties. Bishop compared the compressive strength after impact behavior of an earlier version of a PEEK composite (APC1) with that of carbon fiber/epoxy laminates. She found APC1 had a higher compressive strength after impact although exhibiting a lower strength before (1:295).

Stober, et al, confirmed the general solvent resistance of APC1, and performed dynamic mechanical analysis (d.m.a.), similar to that performed in this research, on both neat resin and single ply reinforced composites (2:1845). They found "a strong correlation" between the α glass transition and the melting transition for neat PEEK in tension and APC1 d.m.a. in flexure (2:1851).

Jones, et al, outlined the mechanical properties further, describing stiffness, toughness, and strength (3:1385). They confirmed that PEEK composites deformed in a nonlinear fashion (as do thermoplastics as a class), but argued this behavior followed "a simple pattern" and that small strain levels (<1%) produced predictable, linear behavior (3:1386). This behavior has been reported in glass-fiber/epoxy matrix composites, too (21:59) (23:378).

A more recent study by Cebel, et al, examined the tensile properties of PEEK films prepared with different thermal histories (4:487). Yield strains for air-cooled specimens (processed at a low quench rate similar to that of the

neat resin sample employed in this research) were 5.5% and 9.0% for test temperatures of 125°C and 25°C, respectively (4:495).

Tung and Dynes characterized the effect of processing conditions on the morphology of APC2, the follow-on to APC1 (5:505). They employed torsion of rectangular samples in their d.m.a. over the temperature range from -120°C to 350°C, but did not vary the dynamic frequency (5:512). The analysis of unidirectional lamina in flexure has some advantages over torsion of rectangular samples. A more unified procedure available for characterizing the mechanical properties of fiber reinforced composites has been shown to be the torsion of thin walled tubes (27:37). However, the rectangular specimen is easier to fabricate, and flexure test is less difficult to control (28:801). Thus the flexure test is more convenient.

This study attempts to predict the complex flexural modulus, $E^*(\omega)$, for an anisotropic laminated beam, as a special case of laminated plate theory. Experiments determined the viscoelastic behavior of a PEEK/graphite fiber composite, available commercially as APC-2. Dynamic three point flexure tests measured the stiffness of thin, unidirectional beams. The results from the analysis are compared to experimental data. Also, frequency-temperature shifting factors obtained from experiments are compared to values predicted from the Williams-Landel-Ferry (WLF) equation.

The Dynastat viscoelastic static and dynamic analyzer was used for the flexural tests. It calculates the loads, complex viscoelastic moduli, and, through a curve-fitting algorithm, obtains the frequency-temperature shift factors. It has a data processing system that produced many of the graphs in this report. The Dynastat was designed to transversely flex long, thin samples of extremely stiff materials. This stiffness might otherwise complicate traditional tensile experiments due to the tensile machine compliance approaching the material's compliance. Typical flexure specimens in this study are rectangular beams approximately 42mm long, 12mm wide, and 1mm thick.

Although the Dynastat measures dynamic flexural viscoelastic properties with some precision, caution must still be used when applying flexural moduli to design problems. The effects of shearing stress in composite laminated structures can be significant and must therefore be examined before a comparison of flexural and tensile moduli can be made. However, when the structure is intended to sustain bending moments, properties obtained from flex tests are of value. The design of structures from polymeric composites which are intended to dampen vibrations also requires viscoelastic moduli.

The goal of this research was to study the effect of matrix viscoelasticity on the mechanical behavior of the PEEK composites, extending the previous research just pre-

sented. Conversely, what effects did the presence of the fibers have on the viscoelastic behavior? A dynamic flexure, rather than tensile, test was selected to achieve this goal because of the high sample rigidity, the need for high machine sensitivity, and the consequent reduction in the applied load.

One of three objectives of this research is to evaluate the flexural test and to account for other effects, i.e., shear and Poisson effects. The chosen analytic model applies a hybrid micro- and macromechanical approach to the analysis of a flexure specimen. An isotropic sample of PEEK resin provided baseline data for the matrix properties. By substituting that frequency-dependent viscoelastic data into relations ordinarily used for predicting the static behavior of homogeneous, anisotropic elastic materials, it was hoped to obtain values that agreed with experimental results. This model is developed in the second chapter of this report.

The second objective of this study was to characterize the frequency and temperature dependency of APC-2 in dynamic flexure. Factors considered were the longitudinal and transverse orientations of the continuous fibers relative to the longitudinal axis of the flexure specimen.

Processing differences, such as quench rate during specimen preparation, were not variables. A single unidirectional plate provided the composite specimens for experi-

mentation. The mid-span displacements were small, intended to keep curvatures small and the strains in a linear range. The third section of this report details the experimental procedures used to determine the material behavior.

A final objective was to compare frequency-temperature shift factors obtained in three ways: analytically, using the WLF equation; experimentally, using the Dynastat curve-fitting algorithm; and manually, using hand-shifted values from experimental results. This comparison, and other results of the experimental work, are discussed in the fourth chapter of this report.

II. Theory

Investigations of the dynamic mechanical properties of polymers have employed torsion, tension, and three-point bending. Flexure of homogeneous viscoelastic specimens has provided reliable data that correlated well with tensile properties (24:9). Because the sample stiffness may approach that of the structural parts of the testing machine, the experimenter who determines the viscoelastic behavior of a stiff composite will often choose flexure as the test method. The analysis of the experiment is then complicated by the specimen geometry, loading and support conditions, as well as any material anisotropy or nonlinearity. For these reasons, bending tests of composites materials are typically limited to quality control and materials acceptance purposes.

This research attempts to model the quasi-static behavior of a dynamic flexure test and account for complications due to the laminated structure of the composite and to the material anisotropy. APC-2 material nonlinearity has already been noted by Jones, but small strains will be assumed in this analysis and enforced in the experimentation.

A precise viscoelastic model will not be developed, i.e., time-dependent constitutive relations will not be used, nor will the elastic solution for the beam bending problem be transformed to the Laplace domain. Inversion from the Laplace domain will thus not be undertaken to

develop time-dependent solutions, because the material behavior in the frequency domain is of interest.

Instead, inertial effects will be ignored and frequency-dependent material parameters will be substituted into the quasi-static elastic beam solution. The model used in this study is built on the analysis of the flexure test for laminated composite materials, proposed by Whitney, Browning, and Mair (6:30). Although their procedure matched tensile properties quite well with flexural characteristics for unidirectional laminates, they warned of its injudicious use for general laminates (6:42). Some factors they considered were free-edge effects, transverse shear deformation, and shear coupling. These factors will be discussed further below. Their findings form a part of the basis of the American Society for Testing and Materials (ASTM) standard test method for flexural properties of unreinforced and reinforced plastics (7:410).

A hybrid micro- and macromechanical approach suggested by Sims and Halpin, and dependent upon the work of Halpin and Tsai, has shown that only one viscoelastic parameter need be measured to predict composite behavior in the glassy region of the resin (11:55). However, they assumed a time-independent Poisson's ratio for the resin below the glass transition temperature (T_g) of the resin. Further development of their approach is required for the flexural response of laminated composites above T_g . This research will pre-

dict APC-2 flexural properties based on matrix and fiber frequency-dependent behavior in a manner similar to the Sims and Halpin rule of mixtures.

Figure 1 depicts the flexure and laminate geometry used in this research. According to Whitney, et al, Hoff showed that the beam's equivalent stiffness, $E_{11_b} I$, could be attributed to the bending stiffness of each lamina, summed over the thickness (6:31):

$$E_{11_b} I = \sum_{k=1}^n E_{11}^{(k)} I^{(k)} \quad (1)$$

where

E_{11_b} = effective bending modulus

I = moment of inertia of the beam relative to the midplane

n = number of laminate layers

$E_{11}^{(k)}$ = modulus of kth layer with respect to the beam axis

$I^{(k)}$ = moment of inertia of kth layer with respect to the midplane

This relation holds for layered beams in which the plies are oriented symmetrically about the midplane and the orthotropic axes of material symmetry in each ply are parallel to the beam edges. Specially orthotropic unidirectional beams are then treated as macroscopically homogeneous.

Whitney, Browning, and Mair continued the approach that Hoff took, and developed the constitutive relations in bend-

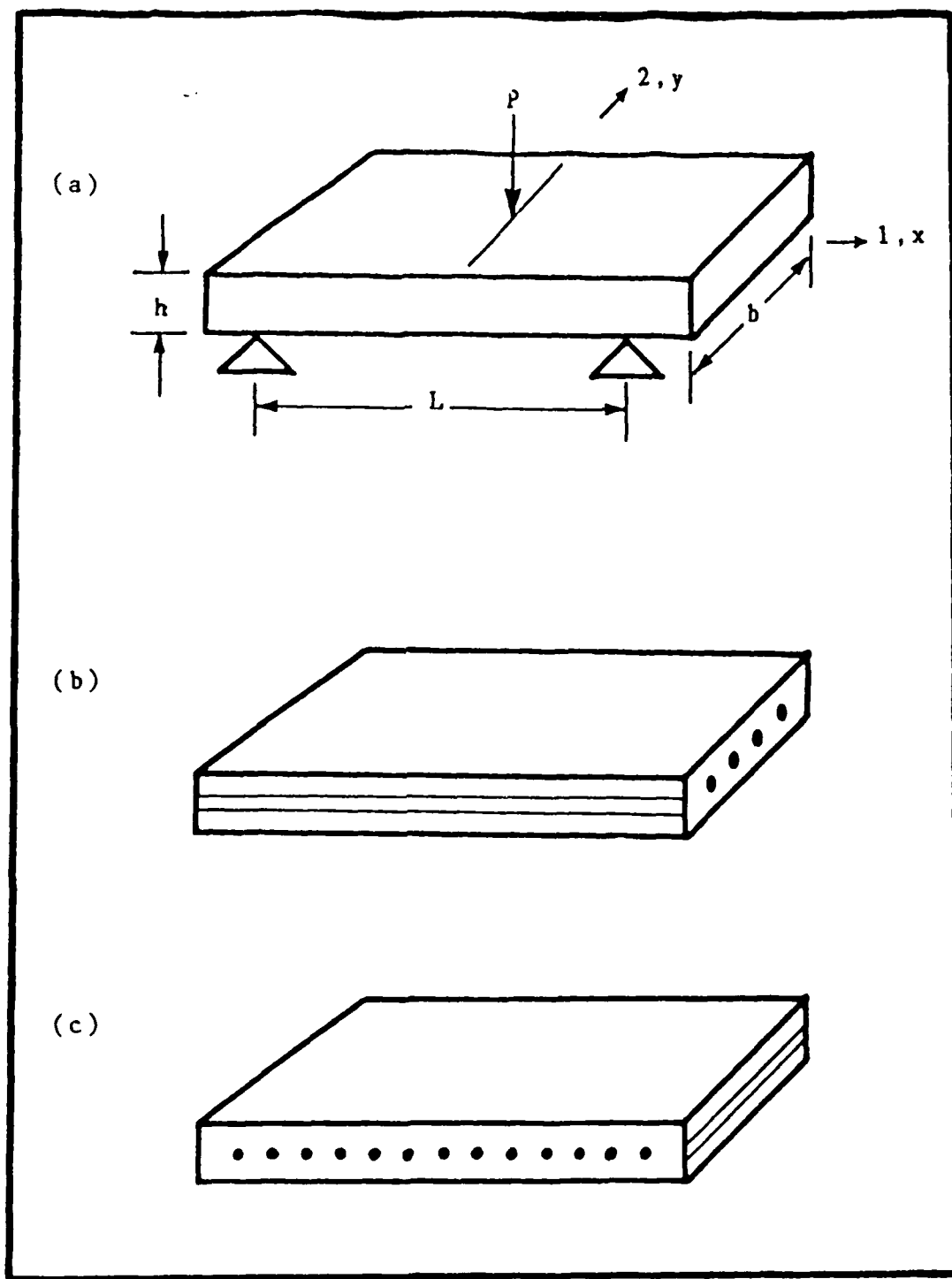


Fig. 1. Three Point Flexure Geometry (a),
 0° (Longitudinal) Sample (b),
 90° (Transverse) Sample (c)

ing. Starting with the constitutive relation for a laminated anisotropic plate in pure bending, assuming no in-plane stress resultants:

$$\begin{Bmatrix} M_x \\ M_y \\ M_{xy} \end{Bmatrix} = \begin{bmatrix} D_{11} & D_{12} & D_{16} \\ D_{12} & D_{22} & D_{26} \\ D_{16} & D_{26} & D_{66} \end{bmatrix} \begin{Bmatrix} K_x \\ K_y \\ K_{xy} \end{Bmatrix} \quad (2)$$

where M_x , M_y , and M_{xy} are the resultant bending and twisting moments per unit length. The plate bending and twisting curvatures are K_x , K_y , and K_{xy} . In unidirectional composites, where the fiber direction is aligned with a plate principal axis, the plate bending stiffness matrix, $[D]$, is not fully populated. Because there are no off-axis plies, $D_{16} = D_{26} = 0$. The inversion of the moment-curvature relation is

$$\begin{Bmatrix} K_x \\ K_y \\ K_{xy} \end{Bmatrix} = [D^*] \begin{Bmatrix} M_x \\ M_y \\ M_{xy} \end{Bmatrix} \quad (3)$$

The D_{12}^* and D_{16}^* elements of the inverse of the stiffness matrix, $[D^*]$, are associated in name with the Poisson effect and shear coupling, respectively.

To neglect the effects of shear coupling, one continues by assuming:

$$M_y = M_{xy} = 0 \quad (4)$$

and that the vertical deflection, w , is a function of x , i.e., $w = w(x)$. This is applicable for beams which have a high length-to-width ratio.

As Whitney, et al, point out, this approach neglects shear coupling. The effect of shear coupling may not necessarily be ignored in angle-ply laminates, and the dependence of the deflection along the y -direction, or width, will cause warping at the beam supports. This research is conducted only on unidirectional beams, and their length-to-width ratio is quite high.

The dependence of the deflection on the width results from the expressions for the curvatures of a plate in terms of the plate deflection:

$$K_y = -\frac{\partial^2 w}{\partial y^2}, K_x = -\frac{\partial^2 w}{\partial x^2}, K_{xy} = -2\frac{\partial^2 w}{\partial x \partial y} \quad (5)$$

Substituting Eqn. (5) into Eqn. (3), and applying Eqn. (4), one obtains the relation showing the effect of Poisson's ratio, D_{12}^* , as

$$\frac{\partial^2 w}{\partial y^2} = -D_{12}^* M_x \quad (6a)$$

and the effect of anisotropic shear coupling as

$$\frac{\partial^2 w}{\partial x \partial y} = - (1/2) D_{16}^* M_x \quad (6b)$$

These effects will be negligible if the ratio of the length to width is large, a normal assumption in beam theory, but sometimes difficult to produce in a flexure specimen. From

Ref. 8, the relation which accounts for shear coupling between the experimentally determined effective flexural modulus, E_{11_b} , and the Young's modulus in the 1-direction, E_{11} , and which produced reasonably good experimental results, is:

$$E_{11_b} = \frac{(L/b)^2 E_{11}}{(L/b)^2 - \nu_{12} (E_{11}/E_{22})} \quad (7)$$

where

E_{11} , E_{22} = Young's moduli in the 1- and 2- directions, respectively

L/b = span-to-width ratio

ν_{12} = Poisson's ratio for the strain in the 2-direction when the beam is stressed in the 1-direction

The ASTM recommendation for the value of L/b is at least 1.6, for the three-point loading of a reinforced plastic flexural specimen with a length-to-thickness ratio of 40 (7:417).

Following the approach Ashton and Whitney took (Reference 22), and that taken by Schultz and Tsai (23:369), Whitney, et al (6:34), expressed the constitutive relations for a homogeneous orthotropic beam in terms of the stresses and strains as:

$$\begin{Bmatrix} \sigma_x \\ \sigma_y \\ \sigma_{xy} \end{Bmatrix} = \begin{bmatrix} Q_{11} & Q_{12} & Q_{16} \\ Q_{12} & Q_{22} & Q_{26} \\ Q_{16} & Q_{26} & Q_{66} \end{bmatrix} \begin{Bmatrix} \epsilon_x \\ \epsilon_y \\ \epsilon_{xy} \end{Bmatrix} \quad (8)$$

where the Q_{ij} are the moduli. This approach is identical to Tsai's transformation of the full stress tensor because there are no off-axis plies (25:440). From an equilibrium study of a laminated plate:

$$\frac{\partial M_x}{\partial x} + \frac{\partial M_{xy}}{\partial y} - Q_x = 0 \quad (9)$$

where the total transverse shear resultant, Q , is $Q = bQ_x$, or, the product of the plate (beam) width and the transverse shear resultant per unit width. Because of the assumption in Eqn. (4), $Q = dM/dx$, where M is the applied bending moment, and is the product of the resultant bending moment per unit width and the plate (beam) width. It is now possible to account for the rotation of beam elements due to shear.

Denoting the normals to the midplane of the beam relative to the x and the y axes, respectively, as ψ_x , and ψ_y , the constitutive equations for plate bending are analogous to the Timoshenko beam theory. Changing Whitney's sign convention to that used by Shames and Dym (30:342), one obtains the curvature-moment relation similar to Eqn. (3):

$$\left\{ \begin{array}{c} \frac{\partial \psi_x}{\partial x} \\ \frac{\partial \psi_y}{\partial y} \\ \frac{\partial \psi_x}{\partial y} + \frac{\partial \psi_y}{\partial x} \end{array} \right\} = - [D^*] \left\{ \begin{array}{c} M_x \\ 0 \\ 0 \end{array} \right\} \quad (10)$$

In shear then,

$$\left\{ \begin{array}{c} Q_x \\ Q_y \end{array} \right\} = k \begin{bmatrix} A_{55} & A_{45} \\ A_{45} & A_{44} \end{bmatrix} \left\{ \begin{array}{c} \partial w / \partial x - \psi_x \\ \partial w / \partial y - \psi_y \end{array} \right\} \quad (11)$$

where the A_{ij} are the resultant anisotropic transverse shear stiffness found from integrating the anisotropic transverse shear stiffness through the thickness, h , of the beam. From equilibrium, $Q_y = 0$. Since $Q = Q_x \times b$, and $A_{45} = 0$, the inversion of the shear relation becomes:

$$\partial w / \partial x - \psi_x = Q / (k \bar{G} b h) \quad (12)$$

where $\bar{G} = 1 / (h A_{55}^*)$, and is the effective shear modulus. A_{55}^* is the 5,5 element of the inverse of the resultant shear stiffness matrix in Eqn. (11). The shape factor k is taken as 5/6, based on elasticity solutions for beams with no crossply angles (8:14). In Eqn. (10), $D_{11}^* = b / (\bar{E} I)$, where the effective bending modulus from Eqn (1) has replaced E . Differentiating Eqn. (12) and substituting the

result into Eqn. (10) produces the governing differential equation for the elastic flexure of a beam:

$$d^2w/dx^2 = (1/k\bar{G}bh)(d^2M/dx^2) - M/\bar{E}I \quad (13)$$

With the applied moment known as a function of x , the elastic deflection can be obtained from the integration and proper use of boundary conditions in Eqn. (13).

For the simply-supported beam under midspan deflection, the maximum deflection, w_o , occurs at the midspan, and is

$$w_o = \frac{PL}{4k\bar{G}bh} + \frac{PL^3}{4\bar{E}bh} \quad (14)$$

where the applied load at midspan is P . Rearranging terms for the effective flexural modulus yields:

$$\bar{E} = \frac{PL^3}{\left(4bh^3 w_o - \frac{PLh^2}{\bar{G}k} \right)} \quad (15a)$$

The net effect of shear deformation is to decrease the calculated value of the bending modulus if shear were ignored. That part of the deflection due to shear can not be measured directly in a flexure test. To calculate the contribution of shear, and attempt to find the part of the effective flexural modulus due only to bending, the measured values of the effective flexural modulus will be increased by including the negative term in the denominator in Eqn.

(15a) to the portion of the denominator without the shear term. The experimental equipment in this research does not account for shear in its automatic scaling of raw data, and instead calculates the effective flexural modulus as

$$E = PL^3 / 4bh^3 w_o \quad (15b)$$

For highly anisotropic materials, the contribution of the second term in the denominator of Eqn. (15a) may be considerable. The effects of this contribution are examined in this research.

Additionally, free edge effects are considered in the model because the state of stress is actually three dimensional in a small zone near the sides of the beam. The stress field can't be considered a plane state for a distance equal to the thickness in from the edges. To minimize the free edge effects, i.e., to approximate a state of plane stress across the majority of the width of the beam, the flexure specimen must have a high width-to-thickness ratio, b/h . ASTM standards recommend $b/h = 25$ for a specimen with a length-to-thickness ratio of $L/h = 40$ (7:417), when that sample is tested to failure.

The maximum dimensions of the Dynastat test chamber, however, forced some experimental trade-offs in terms of specimen geometry. These are discussed in the next chapter. It suffices to say, that in order to obtain measurable results in a regime where small angle approximations and

linear theory are still valid, the nominal b/h value for all flexure specimens in this research is 12.5. Loading did not approach failure loads, and edge delaminations were not observed.

Up to this point in the analysis, the microscopic nature of the composite has been suppressed. To continue, one assumes the matrix of the composite to act isotropically, while allowing the fibers to behave anisotropically. This approach, taken by Halpin and Tsai and reported in Ref. 9, has been called a rule of mixtures approach. The macroscopic composite behavior is assumed to be described by the volume-weighted sum of the behaviors of the fiber and matrix separately. Referring to Figure 1, then,

$$E_{11} = k(E_f V_f + E_m V_m) \quad (16)$$

where

E_{11} = Young's modulus in the 1- direction

E_f, E_m = Young's moduli of the fiber and matrix,
respectively

V_f, V_m = volume fraction of fiber and matrix, respectively

k = fiber alignment factor

The fiber alignment factor is assumed to be 0.9 throughout this analysis. Since the prepreg plies were cut and stacked up by hand, and a value of $k = 1.0$ would describe perfectly aligned fibers, the above factor yields a conservative value.

In the transverse direction, the composite modulus becomes

$$E_{22} = E_m \frac{E_f (1 + \xi V_f) + \xi E_m (1 - V_f)}{E_f (1 - V_f) + \xi E_m (1 + V_f / \xi)} \quad (17)$$

where ξ is the fiber packing factor. This value depends on the spacing around individual fibers and their neighboring fibers. Whitney has shown that the transverse, not longitudinal, fiber modulus should be used for E_f in Eqn. (17) if significant fiber anisotropy is present (17:188). If the circular fibers are arrayed in a square, Hewitt and deMallerbe (10:118) suggested calculating ξ as

$$\xi = 1 + 40V_f^{10} \quad (18)$$

The rule of mixtures applied to the calculation of the Poisson's ratio yields:

$$\nu_{12} = \nu_m V_m + \nu_f V_f \quad (19)$$

Of course, Equations 16 through 19 make no allowance for the frequency dependency of any of the material parameters. This research will employ Eqns. (16) and (17) in a quasi-static manner with flexural properties substituted for the Young's moduli of the fiber and matrix as appropriate. The effect of the viscoelastic nature of the matrix can then be observed on the applicability of the rule of mixtures.

Assuming frequency-independent, elastic, anisotropic graphite fiber properties, and an isotropic matrix, only the matrix material need be modeled by frequency-dependent variables. From Eqns. 6 and 15, with shear deformation neglected, two material properties to be described visco-elastically are Poisson's ratio and the flexural modulus. Temperature dependency will be observed and related to frequency by superposition.

The frequency dependent Poisson's ratio and flexural modulus will consist of in-phase and out-of-phase components. However, an extensive study by Koppelman, reported by Ferry, indicates that "the imaginary component of Poisson's ratio ... is small, perhaps zero" (11:444). Then the matrix Poisson's ratio is $\nu_m = \nu_m^*(\omega) = \nu_m'(\omega)$.

For the harmonic strain excitation to be considered here, the complex modulus, $E^*(\omega)$, is defined as the ratio of the harmonic stress response to the strain. If sufficient time after the application of strain has occurred to neglect the initial conditions, for strain $\epsilon(t) = \epsilon_0 \exp[i\omega t]$, and stress $\sigma(t) = \sigma_0 \exp[i\omega t]$,

$$E = \sigma_0 / \epsilon_0 = E^*(\omega) = E'(\omega) + iE''(\omega) \quad (20)$$

$E'(\omega)$ is the frequency dependent in-phase component of $E^*(\omega)$ (20:24). $E'(\omega)$ is also called either the storage modulus or the real part of the complex modulus. $E''(\omega)$ is called either the out-of-phase, or imaginary, component, or the

loss modulus. The ratio of the out-of-phase to in-phase components is called the loss factor. The loss factor is the tangent of the phase angle, δ , between the components of the complex modulus, i.e., $E''/E' = \tan \delta$. The loss factor is related to the material damping factor (21:56).

When the fibers of a unidirectional composite beam are oriented such that the fibers are parallel with the longitudinal axis, dynamic three point bending determines E_{11}^* (reference Figure 1). Similarly, when the fibers are oriented such that they are transverse to the beam longitudinal axis, dynamic three-point bending determines E_{22}^* .

The important characteristic of materials modeled as thermorheologically simple solids is their frequency-temperature behavior. The flexural modulus at one temperature will exhibit a frequency dependence that graphically matches a portion of the behavior at another temperature. Finite temperature changes produce shifts in the modulus on a logarithmic frequency scale. The Williams, Landel, and Ferry (WLF) equation predicts the amount of this shift as a function of temperature. Experimentally, one obtains the master curve of a material by shifting spectra over the actual frequency range relative to a reference temperature. Thus the behavior of the modulus can be presented relative to a reduced frequency over a wider range of frequencies than actually observed.

The reduced frequency is the product of the actual frequency (at which modulus data was obtained) and the amount of shift, or shift factor. A good approximation of the shift factor, $a(T)$, for a reference temperature, T_R (about 50°C above the glass transition) that holds for many polymers is

$$\log_{10} a(T) = -8.86(T - T_R)/(101.6 + T - T_R) \quad (21)$$

where T is the actual temperature of the measured spectra. Eqn. (21) is the WLF equation. It holds only near and above the glass transition temperature, T_g (11:289).

Quite apart from the empirical curve-fitting technique of horizontally shifting the spectra (or the application of the WLF equation) is another temperature reduction on the complex modulus. This is predicted by Rouse's theory. Ferry reports that this is based on the hypothesis "that the modulus contributions are proportional to ρT " (11:269). The density, ρ , is often dropped. This is acceptable because "it is impossible to distinguish empirically between the merits of ρT and T " (11:271).

Master curves generated in the results section of this report plot the moduli, multiplied by the factor of T_R/T , versus the reduced frequency, $f \times a(T)$, where f is in hertz.

III. Experimental Procedure

Materials

Specimens in this research were cut from a 6 x 9 inch composite plate prepared by hand from multiple plies of PEEK tape pre-impregnated with graphite fiber. This tape, or prepreg, was manufactured by the Fiberite Co., a subsidiary of ICI Americas, Wilmington, Delaware, and was designated APC-2/AS4. Individual plies were 0.005mm thick. Eight ply laminates were prepared in a unidirectional stacking sequence, and processed under temperature and pressure to produce composite specimens from 1.016mm to 1.040mm thick. The processing procedure described below results in composites with properties similar to those listed in Table 1.

Table 1

Typical Mechanical Properties of APC-2 at 25°C

Data from (12:1410) and (3:1388)

Flexural Modulus, GPa	134
Longitudinal Tensile Modulus, GPa	124 - 141
Transverse Tensile Modulus, GPa	8.9 - 10.3
In-Plane Shear Modulus, GPa	4.0 - 6.27
ν_{12}	0.38
ν_{21}	0.04
Melting Point, °C	345

The composite processing followed the thermal history optimized by the Fiberite Co. (13), and was conducted at the Air Force Materials Laboratory Non-Metallics Division, Structural Materials Branch. The prepreg plies were placed in a mold press under a light, contact pressure. The press platens were heated to 385°C from room temperature in 60 minutes. Platen pressure was then increased to 200 psi, and maintained for 45 minutes at 388.1°C +/- 5.0°C. A slow quench rate period followed, still under high pressure, from 391°C to 46°C for 85 minutes.

The average quench rate was -4°C/min. This produces a degree of crystallinity, by density, of about .45 - .48 (5:511). The degree of crystallinity is a measure of order of the polymeric matrix, with an amorphous state having zero crystallinity. Nonlinear viscoelastic behavior has been observed with increasing crystallinity. Other measured properties are listed in Table 2. An acid digestion technique determined the volume fractions.

Table 2
APC-2 Morphology

Specific Gravity	1.607
Fiber Volume Fraction	0.6401
Matrix Volume Fraction	0.3465

Quality control measures included a microscopic study of a sample cross-sectional area of the plate, at magnifications up to 1000x, and an ultrasonic scan at 3.5dB. No significant internal voids or delaminations were observed, although the sum of the volume fractions indicates a void content of less than 2%.

Flexure samples were cut from the plate to nominal dimensions of 2 x 1/2 inches. Samples with the fibers aligned with the length are termed "0°" specimens, while "90°" beams have the fibers oriented with the width. A water-cooled, diamond blade saw cut all specimens, and some edges were wet sanded to final shape, but only along the lengthwise direction, in accordance with ASTM D 790M (7:411). Neither the upper nor lower surfaces were machined. The orientations of the 0° and 90° samples with respect to the three point flex test are shown in Figure 1.

Neat resin samples were prepared from molding several layers of 5 mil thick PEEK film in a high temperature press. Temperatures and quench rates were nearly identical to those for the composite laminate, although the pressure was only 50 psi at the high temperature. A nominal specimen thickness of 2mm was obtained. A typical Young's modulus value of 2.6 GPa was supplied by the manufacturer, ICI, for the non-crystallized Stabar K film (14:1). Cebe, et al, have reported mechanical properties of crystallized PEEK films from 0.005cm to 0.010cm thick. For a similar thermal his-

tory as in this research, their values for Young's modulus were from 1.4 GPa to 2.0 GPa, with a degree of crystallinity of about 0.32 (4:490). Differences between composite and neat resin behavior were thus expected to occur due to the contributions of the fiber to the rigidity and to crystal formation.

Both the Dynastat flexure supports and its environmental chamber determine the maximum allowable specimen widths and lengths. For three-point bending, the maximum specimen width is 0.5 inches. The inner diameter of the environmental chamber is approximately 3 inches. The span of the lower support is 41.71 mm, so most specimens were sized just above this length.

For highly anisotropic laminates, the minimum length-to-thickness ratio should be at least 40, with 60 recommended by the ASTM in reference 7. Shear deformation otherwise will be significant. For the Dynastat support span, this higher value prescribes a sample thickness below 1mm. A standard sample geometry is desirable for both fiber orientations and for the neat resin flexure specimen. It is felt that a sample thickness less than 1mm would lower the stiffness of the 90° and neat resin specimens to the point that the load cell would have difficulty distinguishing force levels from noise during high temperature flexure. Another desirable test parameter is a small maximum center span deflection that produces a small maximum outer fiber

strain. This would not be possible with extremely thin, flexible specimens. Thus a trade-off was made. A relatively low width-to-thickness ratio, 12.5, was used, but the length-to-thickness ratio of 40 was thought to be acceptable. The length-to-width ratio of 3.33 is double the recommended value of 1.6 and further minimizes the effect of shear coupling. This effect is calculated and presented in the results chapter.

Prior to testing, all specimens were stored in dehumidifiers. The size of each specimen was measured just prior to testing, in accordance with ASTM 790M-84 specimen conditioning standard 8.1. These geometric values were necessary inputs to Dynastat automatic scaling functions described below.

Test Equipment

The viscoelastic characterization studies were performed on an instrument commercially available from Imass, Inc., Hingham, Massachusetts, and known as the Dynastat. The system is fully automated for data acquisition and reduction. The five main components of the Dynastat (the servo controller, the Dynatherm, the Dynalyzer, the Data-lyzer, and the test frame) are illustrated functionally in Figure 2, and described below.

The test frame consists of an environmental chamber, a vertical push-pull rod with specimen supports, two displace-

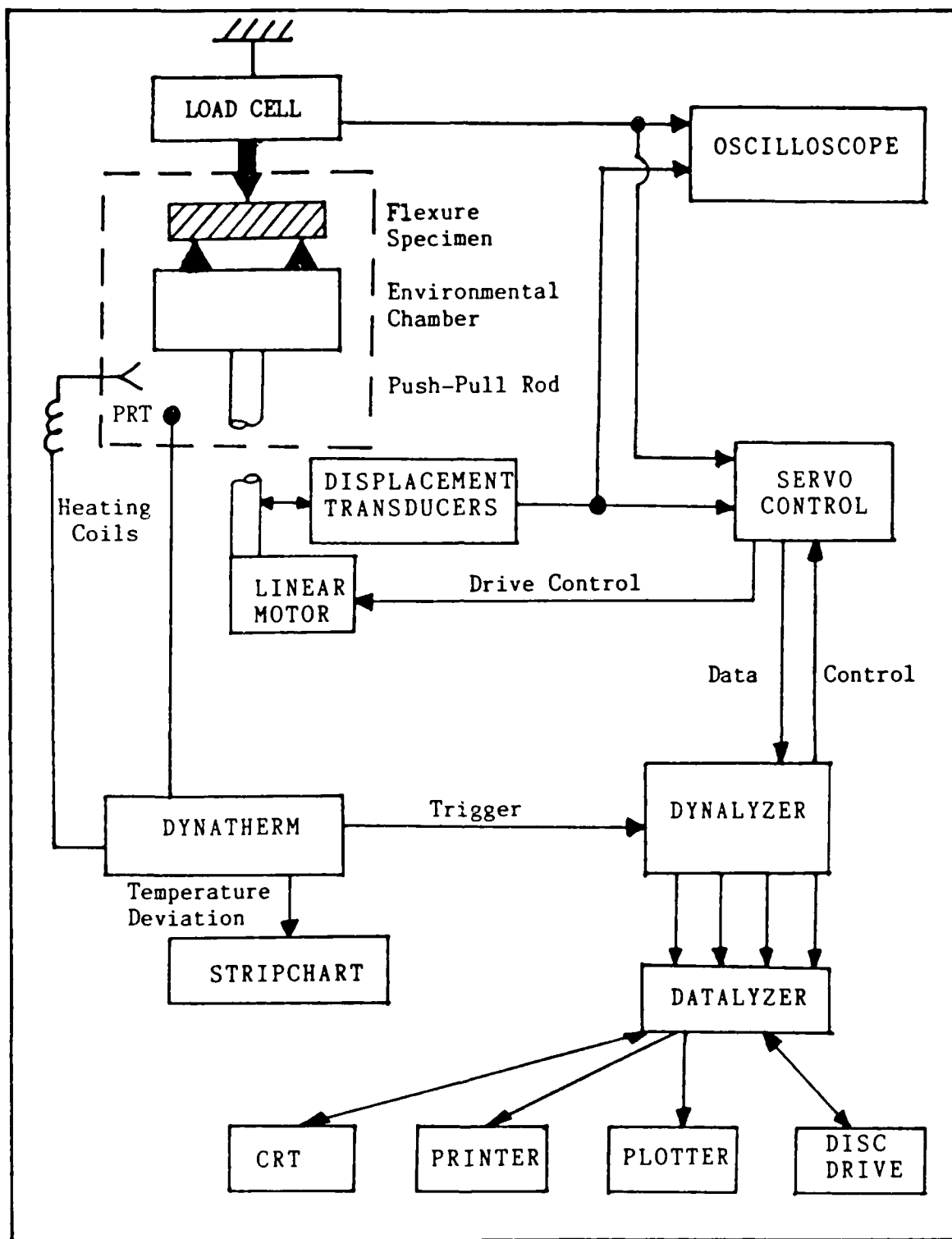


Fig. 2. Functional Relationship of Dynastat Components.

ment transducers, and a load cell. In this study, the low range displacement transducer provides both measurement of and control of the vertical displacement of the lower support. The transducers are below the sample, outside the chamber. A fixed indenter is positioned above the flexure sample. The load cell is above the sample, and is outside the chamber.

All flexure tests were performed using three point loading. The static indenter and the moving lower supports have a load point diameter of 5.0 mm.

The push-pull rod is rigidly coupled to the coil of a linear motor underneath the chamber, and is mounted in an air bearing for transverse stiffness. The linear motor consists of a permanent magnet and a spider suspended coil wound on a lightweight coil form (15:133).

The controlling servos for the linear motor are located in the sub-unit known as the Dynastat (the manufacturer refers to the entire test ensemble by that same name. Unless specific mention is made to the servo controller, further references to the Dynastat include the ensemble). The servo system provides closed-loop control using the displacement transducer for feedback (15:135). The push-button potentiometers on the servo controller "operate logic switches which permit ... step function inputs of ... displacement and ... dynamic external inputs" (16:6). The experimenter programs the static and dynamic amplitudes into

the servo controller and then includes timer inputs, dynamic signals, and thermal triggers into the test by adjusting the other sub-units of the ensemble.

Temperature control of the environmental chamber is provided by the Dynatherm. The Dynatherm also programs temperatures increments and provides thermal triggers to the servo controller. Thumbwheel settings on the front of this sub-unit define the lower and upper temperature setpoints, and the number of intervals between them. Up to 99 intervals can be programmed into the temperature range of between -150°C and 350°C (18:2).

The Dynatherm controls the heating of forced air through the environmental chamber by sensing chamber temperature with a platinum-resistance thermometer (PRT) and servo controlling the heater. The control logic is a mixture of proportional and integral control, and provides temperature stability of $\pm 0.1^{\circ}\text{C}$. Typical response for a programmed 5°C increment is shown in Figure 3. Figure 3 is a portion of a stripchart history recorded for a calibration run. The vertical axis represents temperature deviation from the setpoint. The horizontal axis represents time, illustrating that dynamic data collection sweeps were conducted at the end of a stable time soak.

The PRT is placed near, but not in contact with, the flexure sample in the chamber. No thermocouples are attached to the specimen. The soak time is intended to insure

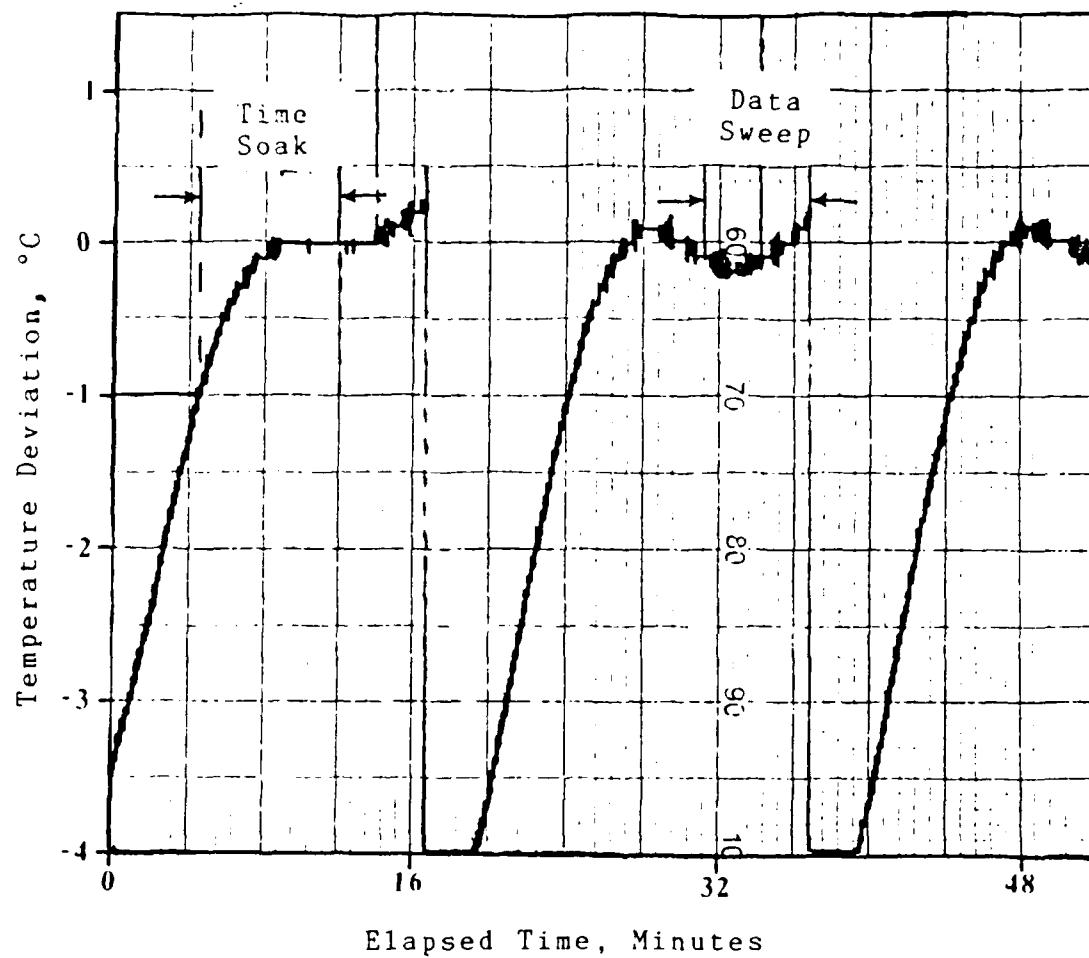


Fig. 3. Thermal Stability of the Dynastat Chamber For 3 Steps

that the sample temperature is as close as possible to the temperature of the chamber air.

Dynamic control and signal correlation is provided by the Dynalyzer. The Dynalyzer and the Dynatherm cooperatively provide automatic temperature and frequency sweeps. The Dynalyzer digitally generates a harmonic signal that drives the linear motor, and which serves as the reference for in-phase and out-of-phase component matching. The Dynalyzer obtains complex moduli values using a modified Fourier transform and auto-correlation process that compares the load cell and displacement transducer outputs with the reference signal. The frequency range of the Dynalyzer is from 0.1 Hz to 199.9 Hz, with a maximum error of ± 0.016 Hz in the range from 0.16 Hz to 15.9 Hz used in this research. The range of measurement for the loss factor, or $\tan \delta$, is from 0.001 to 19.999 (19:4).

The Dynalyzer furnishes four digital values (raw data in units of volts/volts) to the Datalyzer for storage in a data array. These are the unscaled loads and displacements, and the unscaled in- and out-of-phase components of the load relative to the displacement. The Datalyzer is a microprocessor-based instrument which contains a random access memory (RAM). The read-only memories (ROMS) of the Datalyzer permit it to communicate with peripheral devices including a printer, a plotter, and a floppy-disc drive. The utility of these devices is discussed later.

The Datalyzer manipulates the raw data with geometry factors, load and displacement scales, and several correction factors such as machine compliance. These factors are entered by keyboard. In displacement control mode, the Datalyzer calculates $E^*(\omega)$ from the relation for an isotropic, homogeneous beam without shear, i.e., from Eqn. (15b). The Datalyzer output can be printed in real time, or stored on floppy diskette for later analysis. The ROMS provide the capability to plot the results of the dynamic tests against appropriate frequency or temperature scales.

The Datalyzer assigns an eighth-order polynomial to the moduli data at each temperature as a function of the actual frequency. The Datalyzer then computes the shift factors for each spectrum with respect to the spectra at the next higher and lower temperatures. First the Rouse theory, or temperature correction, is applied to the moduli. Then the minimum integral area under adjacent polynomials is calculated. Each calculation results in $a(T)$ for that temperature.

A real time check on the operations of the Dynastat is provided by an oscilloscope. The oscilloscope displays the output waveforms of the load and displacement channels during frequency sweeps. This function is necessary to ensure the indenter remains on the specimen at all times. Clipped sine waves on the load trace indicate that the indenter has risen off the specimen, and that the indenter

requires readjustment. Also, the noise in either channel is visually evident at any time during test runs. This visual monitoring of the waveforms was essential to determining the magnitudes of the static and dynamic programs on the servo controller. Later, the monitoring was essential to determining the quality of the resulting data.

Experimental Method

The viscoelastic data in this study resulted from dynamic flexure only. However, before a dynamic test was conducted on a given ply orientation or on the neat resin specimen, the linearity of the static load-displacement relation had to be determined at several temperatures within the expected range of the dynamic test. In addition, an optimum ratio of the static to the dynamic deflections had to be determined. Obviously, the amplitude of the maximum dynamic deflection had to be less than the static load, or the indenter would rise off the sample. But the need for a high signal to noise ratio was the primary reason for determining the static-to-dynamic displacement ratio.

During static load-displacement tests, the sample was loaded in flexure, and the displacement was stepwise increased to 0.1% strain, as calculated from the relation for the ASTM standard:

$$\epsilon = 6hw_0/L^2 \quad (22)$$

No strain gauges were placed on the sample. Experimental data from Whitney, et al (6:38), and Srinivasan, et al (26:279), revealed little difference in measured bending stiffness compared to the method of displacement measurement used here. The maximum outer fiber strain of 0.1% is well below the ASTM recommended limit of 5% due to flexure (7:411).

These incremental deflections were repeated at elevated temperatures, and the output of the load cell and the displacement transducer was recorded. The results are discussed in the next chapter.

The maximum dynamic displacement was determined by a preliminary dynamic test, the purpose of which was to find an optimum signal-to-noise ratio (S/N) in the load channel. As the sample softened with increasing temperature, S/N could be expected to worsen, degrading the accuracy of the auto-correlation process of the Dynalyzer. All dynamic mechanical tests were then conducted at this deflection ratio. This ratio, and its relation to the static load-displacement response, are discussed in the next chapter.

The temperature/dynamic mechanical tests were conducted after machine calibration and sample geometry factors were entered into the Datalyzer. This entry was required only at the start of the test. With the exception of the neat resin sample, all frequency sweeps were conducted at discrete frequencies in a two decade band from 0.16 Hz to 15.90 Hz (1

rad/sec to 100 rad/sec). Neat resin measurements were attempted at the same frequencies, but only the data at four discrete frequencies between 2.5 Hz and 10.09 Hz were of any value due to noise. The sweep (and data collection period) for all samples started 7.0 minutes after the environmental chamber temperature reached $\pm 1.0^{\circ}\text{C}$ of the programmed temperature.

The chamber temperature ramped up after each frequency sweep in 10°C steps for the composite samples, but to only three setpoints for the neat resin. No cryogenic tests were run, but rather the temperature ranges were typically from near ambient to about 250°C .

The Dynalyzer averaged the Dynastat output over 10 to 15 cycles at each frequency to further increase noise discrimination. An improper assumption that data at the low temperatures, or glassy region, would not be as noisy led to the use of 10 cycles versus 15 cycles in that region. This assumption resulted in noisy data in this region, although much of the scatter may be attributable to composite behavior.

After transmitting the averaged data to the Datalyzer, the Dynalyzer advanced to the next driving frequency, while the Dynatherm ensured chamber temperature stability. The Dynalyzer delayed accepting digital data from the Dynastat at any new frequency for an adjustable time period. This delay equaled one cycle for frequencies less than 1.0 Hz,

and equaled 1 second for frequencies at and above 1.0 Hz. The delay ensured transients had damped out after the increase in driving frequency.

An entire frequency sweep, conducted over fifteen cycles for eleven discrete frequencies at one temperature, took approximately five minutes. Heating to the next temperature took approximately twelve minutes (this time increased at higher temperatures). After a seven minute soak, the sweep was conducted. Usually an eight hour period was required to ramp up to all temperatures and conduct sweeps at each one.

Post test procedures included data transmission from RAM to disk and scaling of the plotter axes from the range of recorded data. Shift factors for frequency-temperature superposition were calculated. The resultant master curves were plotted for the composite samples only.

IV. Results

Before the major findings of this research are explored, the results of the static load-displacement tests will be presented. Those results defined the region of the dynamic sweep, that is, the static-to-dynamic displacement ratio. The temperature dependence of $E'(\omega)$, $E''(\omega)$, and the loss factor, $\tan \delta$, will then be presented. Frequency-temperature shift factors are next presented and compared. The frequency-temperature transformation is only applicable near or above T_g , therefore the shift factors in this research are examined only in that temperature region. Master curves, generated by the frequency-temperature superposition of individual spectra, are presented, and compared by shift technique. Experimental results are compared to the theoretical predictions for shear deformation effects, shear coupling, and volume fraction contributions.

The results of the static deflection tests are depicted in Figures 4 and 5. Figure 4 plots the load cell output (P) as a function of the maximum displacement (w_0) of the push-pull rod for the 90° specimen. This composite demonstrates a linear $P - w_0$ relation in a temperature range of $24.4^\circ\text{C} < T_g < 250.3^\circ\text{C}$. The maximum deflection corresponds roughly to a maximum outer lamina strain of 0.1%, as calculated by Eqn. (22). This calculation ignores inertial effects and includes both static and dynamic deformation.

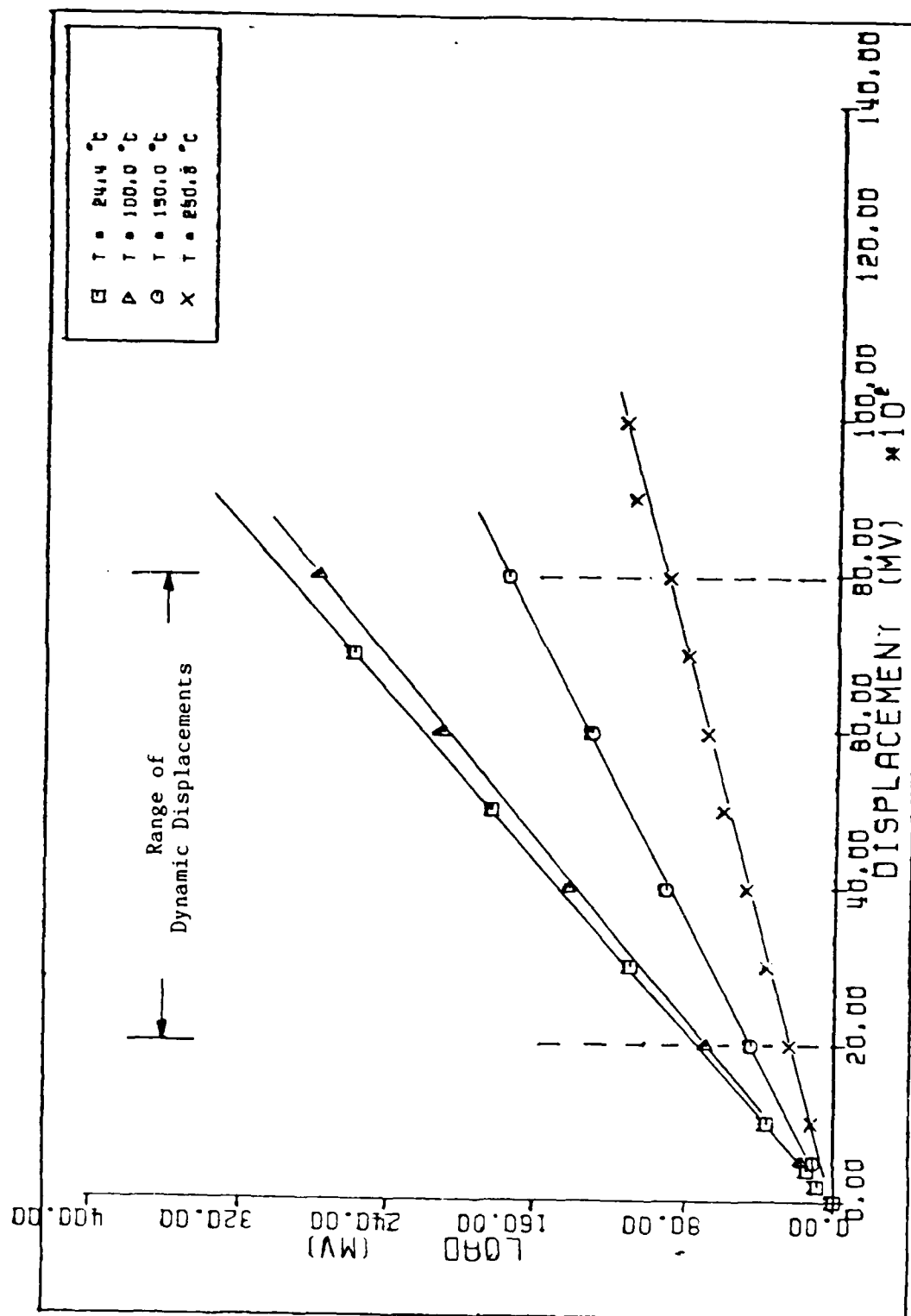


Fig. 4. Static Flexural Response of a 90° Unidirectional APC-2 Specimen

A similar response is shown in Figure 5 for the neat resin specimen. This response correlates well with the nearly temperature-independent linear tensile response observed by Cebe for PEEK films below strains of 1% (4:495).

The regions of the $P - w_0$ curves used for dynamic displacements are also outlined in both figures. In neither case did the total of static and dynamic displacements exceed the linear region. Extensive pretest flexure tests determined the best S/N ratio for the 90° beam. This optimum value was obtained with a static to dynamic displacement ratio of about five to one. The static displacement applied to 90° samples was 0.25mm, which resulted in a low-range displacement transducer output of 5 volts. This is the center of the dynamic range depicted in Figure 4. Similar tests were conducted for the 0° beam and neat resin samples, resulting in static to dynamic displacement ratios of five to three for each.

Initially, the dynamic mechanical behavior of the two unidirectional composites will be presented here separately for the sake of clarity. The first to be discussed will be the matrix-dominated geometry, i.e., the 90° specimen. However, a word on notation is first required.

Note that in Figure 6, and all other plots generated by the Dynastat, the in-phase, or storage modulus, is labeled as M' , not E' . The Dynastat reserves the symbols E' and E'' for unscaled stiffness. The units of M' and M'' are

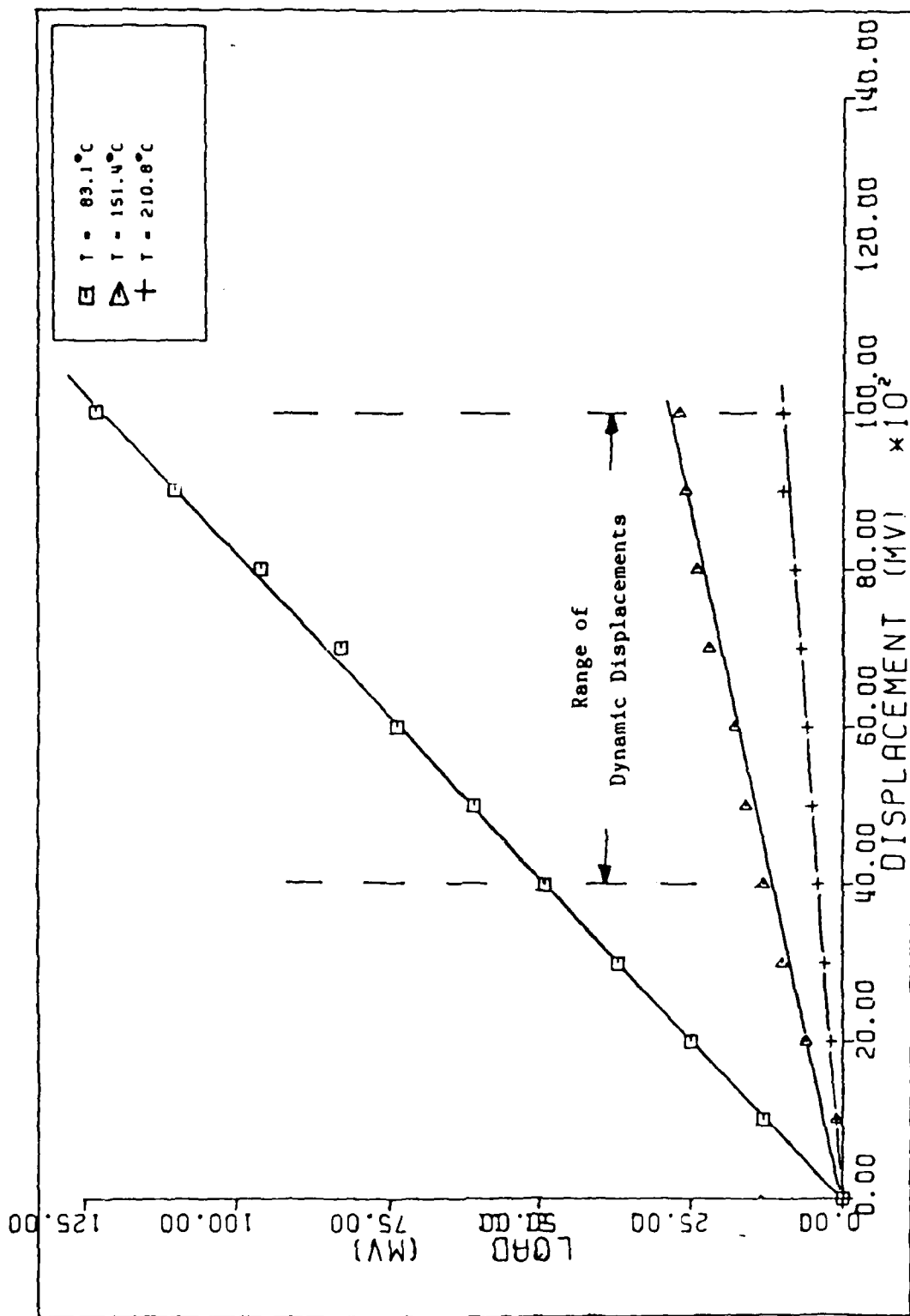


Fig. 5. Static Flexural Response of a PEEK Beam

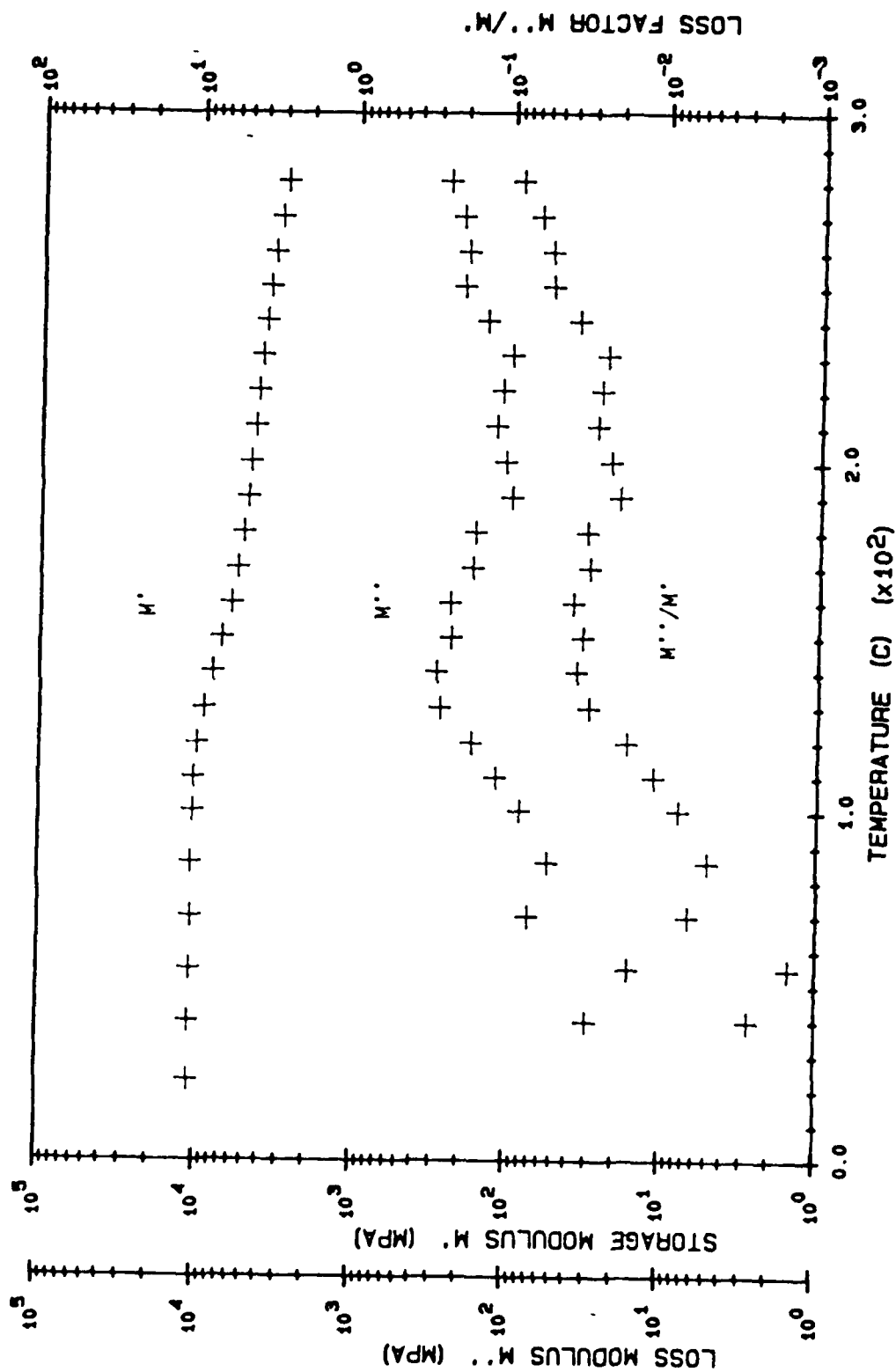


Fig. 6. Temperature Dependency of the Complex Flexural Moduli of APC-2 90° Specimen, 1 rad/sec

identical to those of E' and E'' from Eqn. (20). Of course, the dimensionless loss factor, $\tan \delta$, M''/M' , or E''/E' , is the same regardless of notation.

Transverse (90°) Behavior

The 90 sample underwent three-point flexure from 23°C to 280°C. The temperature response at 1 rad/sec is depicted in Figure 6. For the same specimen and test, the responses at the frequencies of 10 rad/sec and 100 rad/sec are presented in Figures 7 and 8. The following descriptions apply to all three frequencies.

The in-phase component is seen to remain fairly constant with temperature until 120°C. A β transition may occur between 40°C and 70°C. More likely, this is noise. In the glassy region, the in-phase component is very large, and the loss modulus is extremely small. Because of this, $\tan \delta$ approaches the machine lower measurement limit. Data in this region is thus more susceptible to noise and the scatter in the small loss modulus values represents noise more than a material effect.

The loss modulus values reach a broad and shallow peak in the transition region. The out-of-phase response beyond the transition region declines, and then increases as the temperature nears the crystalline melt temperature of 305°C observed by Tung and Dynes (5:508). In this rubbery region, the storage modulus is seen to steadily decline.

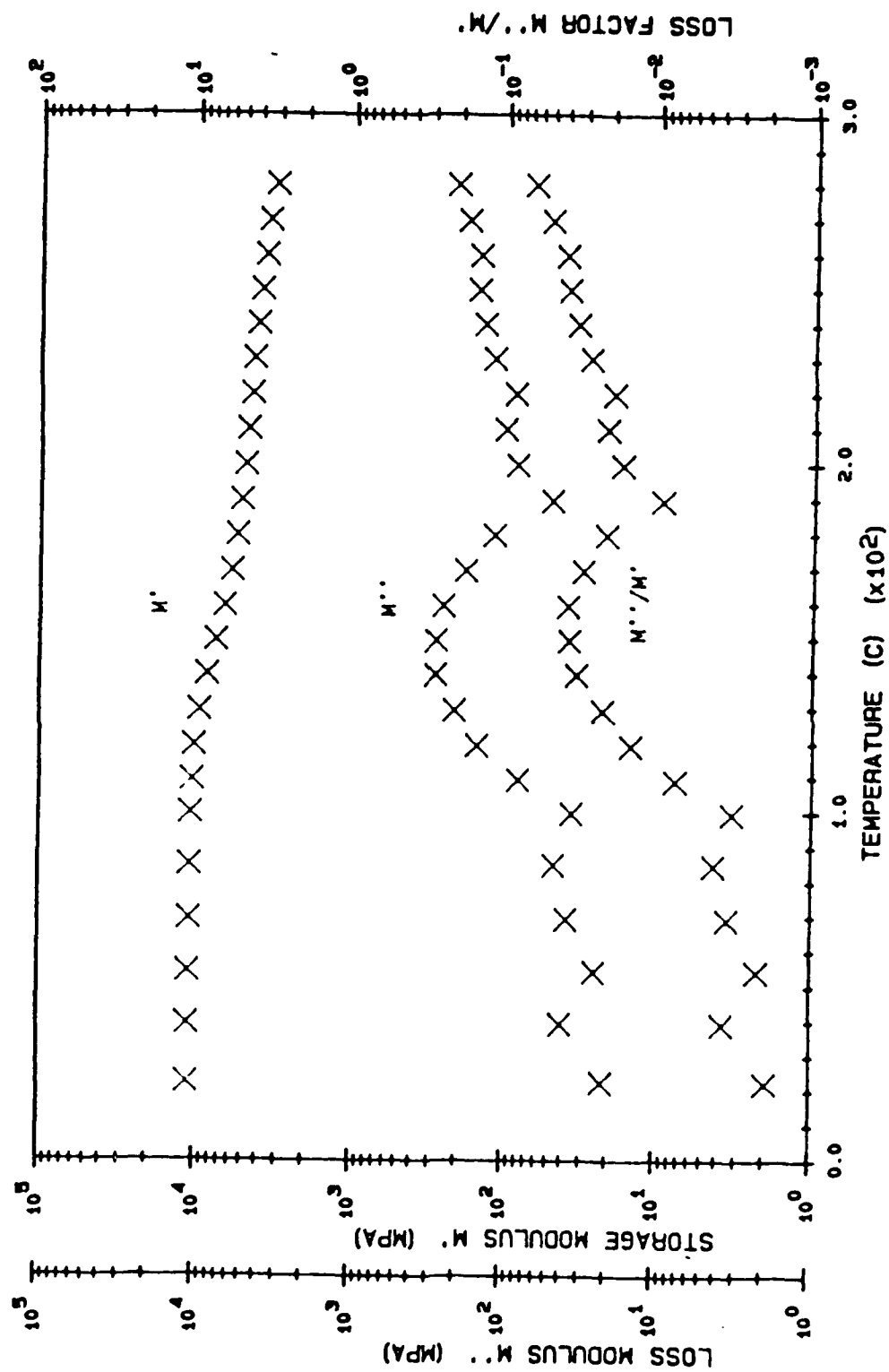


Fig. 7. Temperature Dependency of the Complex Flexural Moduli of APC-2 90° Specimen, 10 rad/sec

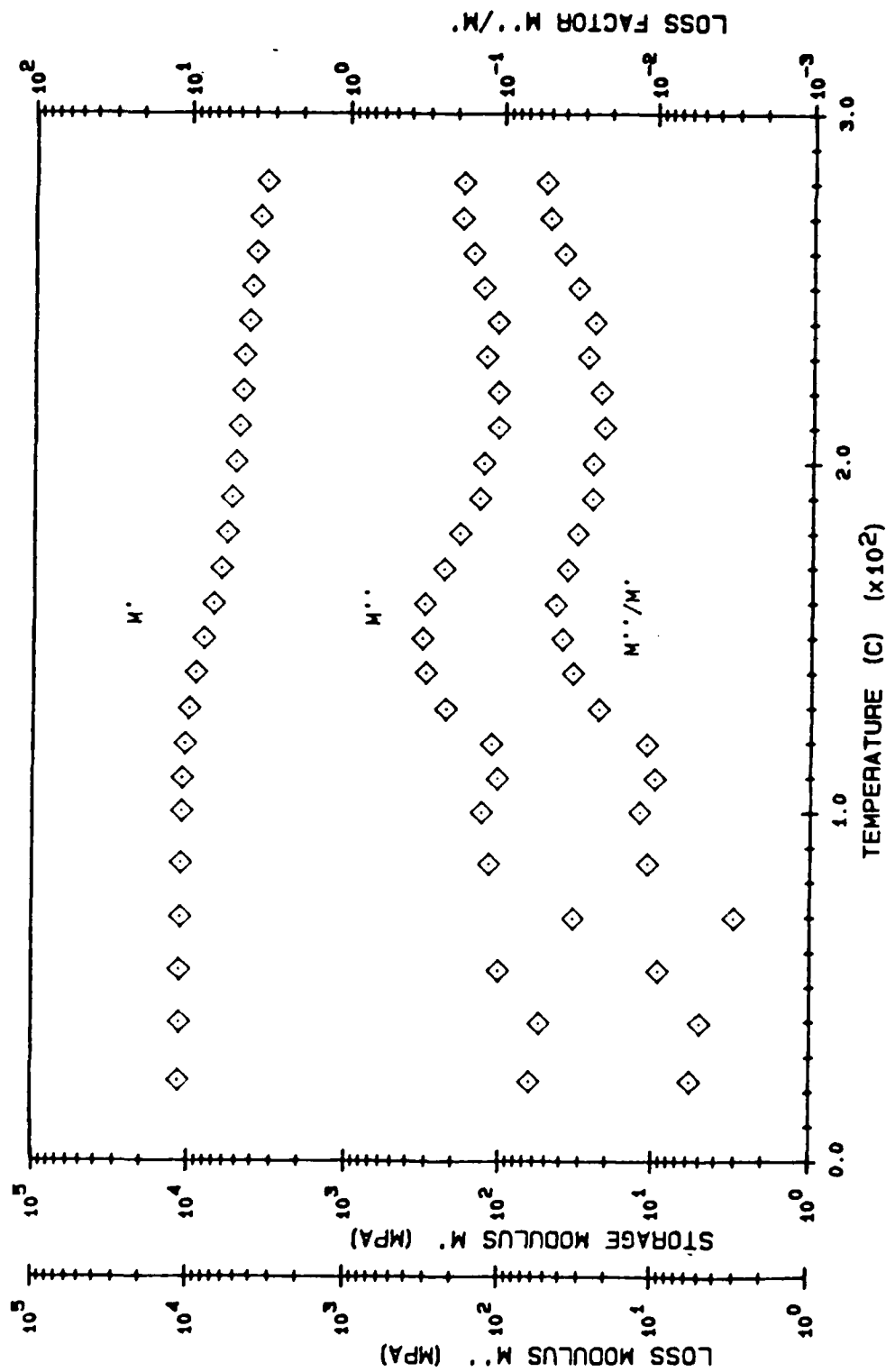


Fig. 8. Temperature Dependency of the Complex Flexural Moduli of APC-2 90° Specimen, 100 rad/sec

Shift factors for the 90° specimen are displayed in Figure 9, relative to the reference temperature of 210.4°C. The shift factors will vary with reference temperature, of course, but Figure 9 indicates that they also depend on which variable (M' or M'') is shifted. Those calculated by the Datalyzer are labeled "Super" because that is the software command required by the Datalyzer to begin shift factor calculations.

Figure 9 shows shift factors calculated by other means, too. Those labeled "WLF" were calculated from Eqn. (21). Those shift factors labeled "Hand" were determined manually by plotting individual spectra and passing them across a scaled light table. It is estimated that the precision of the manual shifts due to the grid size is no better than 3%. Due to inexperience and the difficulty with visually minimizing the area between two overlapping curves, the typical accuracy is close to 20%.

Because of the inaccuracy of the manual method, and due to the possible poor fit of the polynomial spline at the edges of individual spectra, trends, and not values, should be compared in Figure 9. The WLF equation was applied with "universal" constants. No attempt was made to calculate new constants, unique to APC-2, in the WLF equation from slope and intercept values.

The general trend of the experimental shift factors, corresponding to the storage modulus, whether curve-fit by

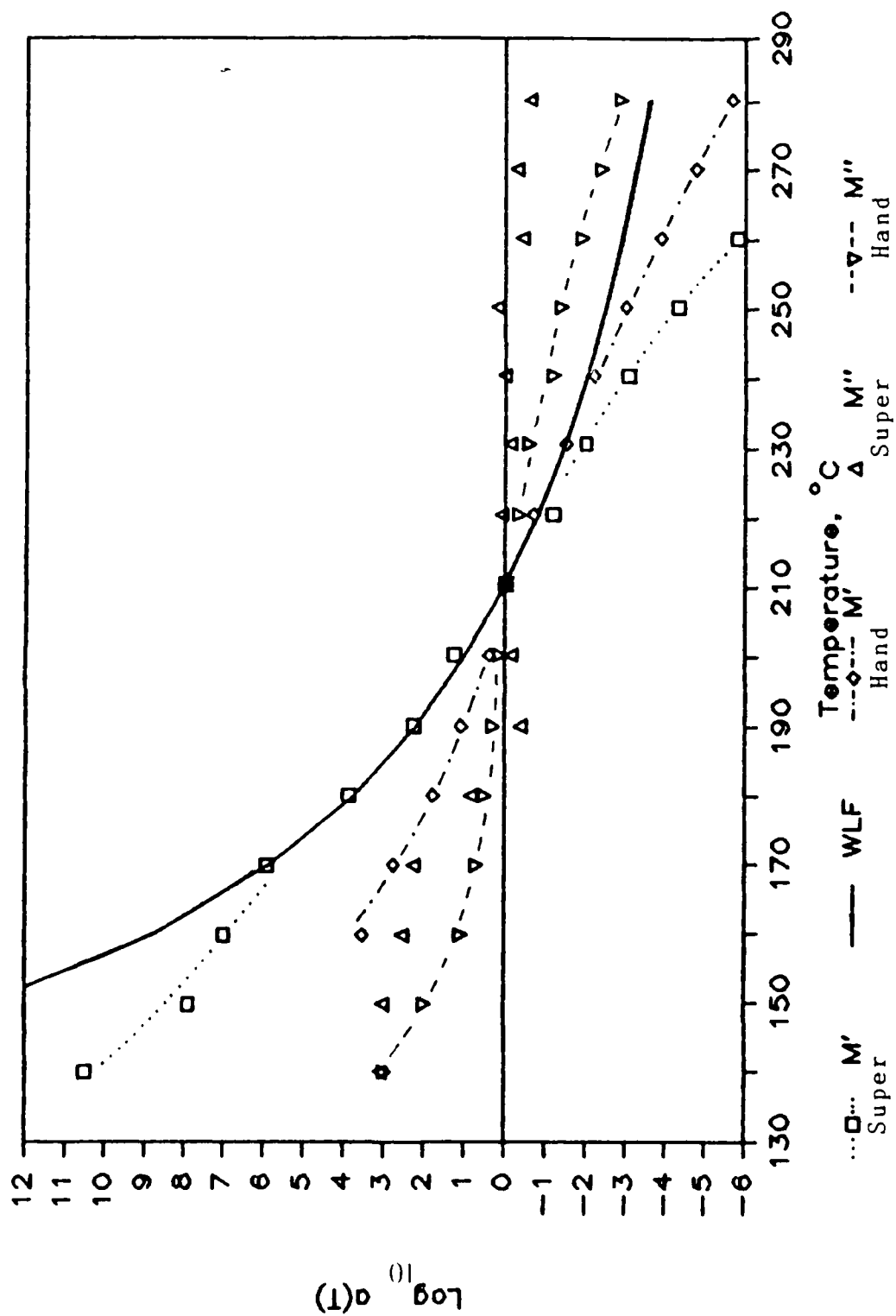


Fig. 9. Effect of Reduction Technique on 90° Specimen Shift Factors

hand or by the computational method of the Datalyzer, shows agreement with a thermorheologically simple solid that the WLF equation models. The leveling of the $\log_{10} a(T)$ at lower temperatures indicates that the WLF equation, as fit to this data, should be modified to include an energy term, similar to an Arrhenius expression for the activation energy (11:290).

The factors based on shifts of the loss modulus are small, and "Super" has difficulty detecting any trend. This is thought to be due to the noisy and relatively featureless loss modulus spectra. The curve-fitting algorithm of the Datalyzer is probably too sensitive to large changes in amplitude or to large differences in the slopes at the ends of the splines. Hand shifting was extremely difficult.

Longitudinal (0°) Behavior

Returning to the discussion of the fiber dominated, or 0° , specimen, Figure 10 displays the temperature dependency of the composite over the range from 80°C to 230°C . Two attempts to obtain data at higher temperatures were thwarted, once due to mechanical problems, and once to a loss of RAM data. Note the difference in the vertical scaling between the loss and storage moduli, chosen for convenience.

As expected, the storage modulus is extremely high, two orders of magnitude above the out-of-phase component, and shows little temperature or frequency dependence. A transition region for the storage modulus is barely apparent on

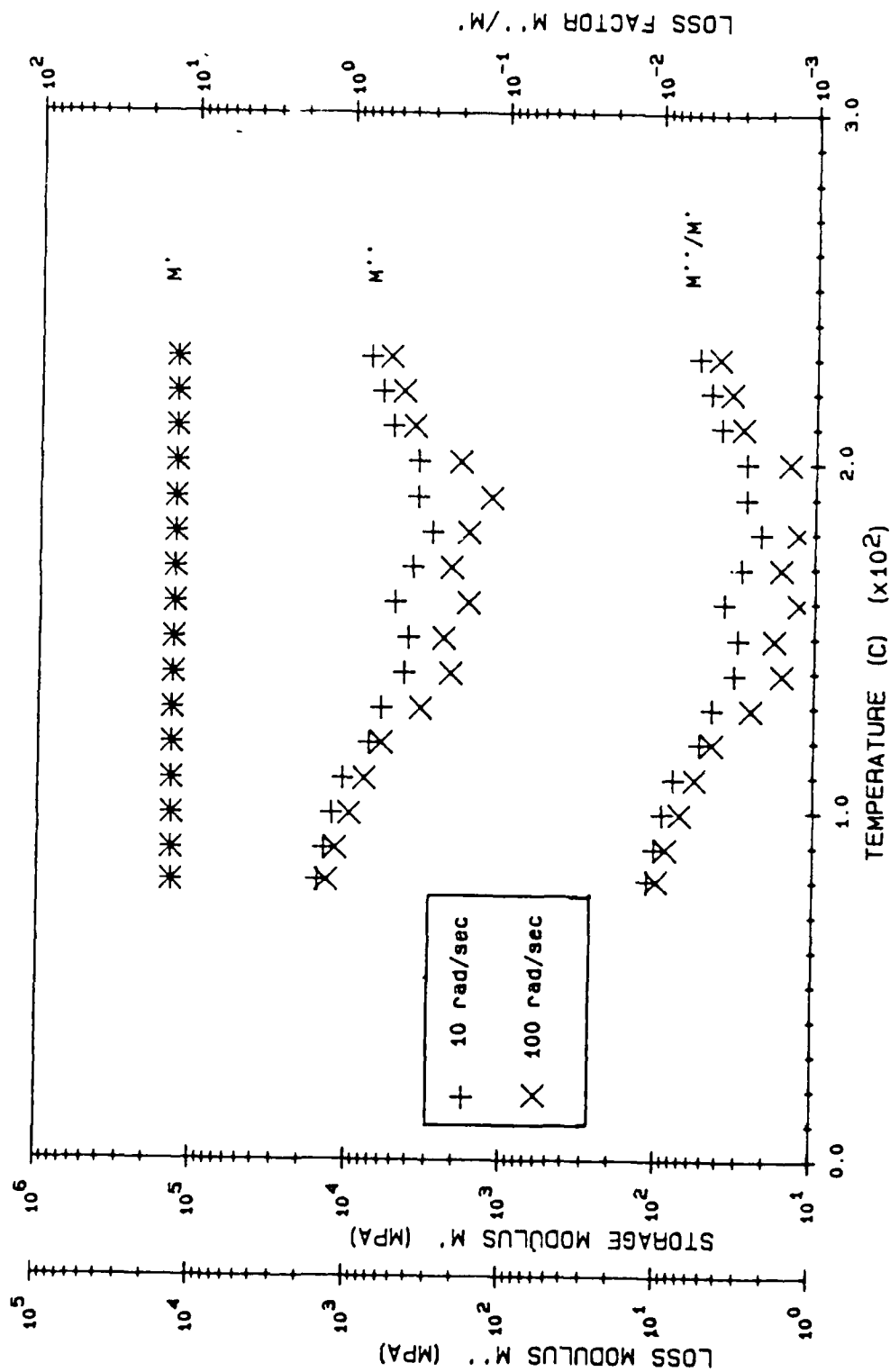


Fig. 10. Temperature Dependency of the Complex Flexural Moduli of APC-2 0° Specimen

the scale of Figure 10. Over the entire temperature range, the storage modulus decreases by less than 4%.

The most striking feature of the fiber dominated behavior, however, is the depressed region around T_g for the loss modulus. Only the smallest peaks above this "valley" are discernible at either frequency shown in Figure 10. The trend above this transition range, though, matches the behavior of the 90° sample in that the loss factor continues to rise with temperature. Significantly, the loss factor is typically an order of magnitude less than that of the 90° sample.

The shift factors generated from the spectra of the 0° specimen are displayed in Figure 11 as a function of temperature, again with respect to a reference of 210°C . The polynomial fit of "Super" exaggerates the shift factor for the storage modulus at several points, but matches the WLF curve more closely than the hand fit. Hand-shifting was extremely difficult due to the small changes in slopes and magnitudes of individual spectra, but yielded a master curve with better continuity over a larger shifted spectrum. The master curve will be discussed below. As with the 90° beam, shift factors based on the loss modulus are small, and their trend is flat, regardless of the technique employed.

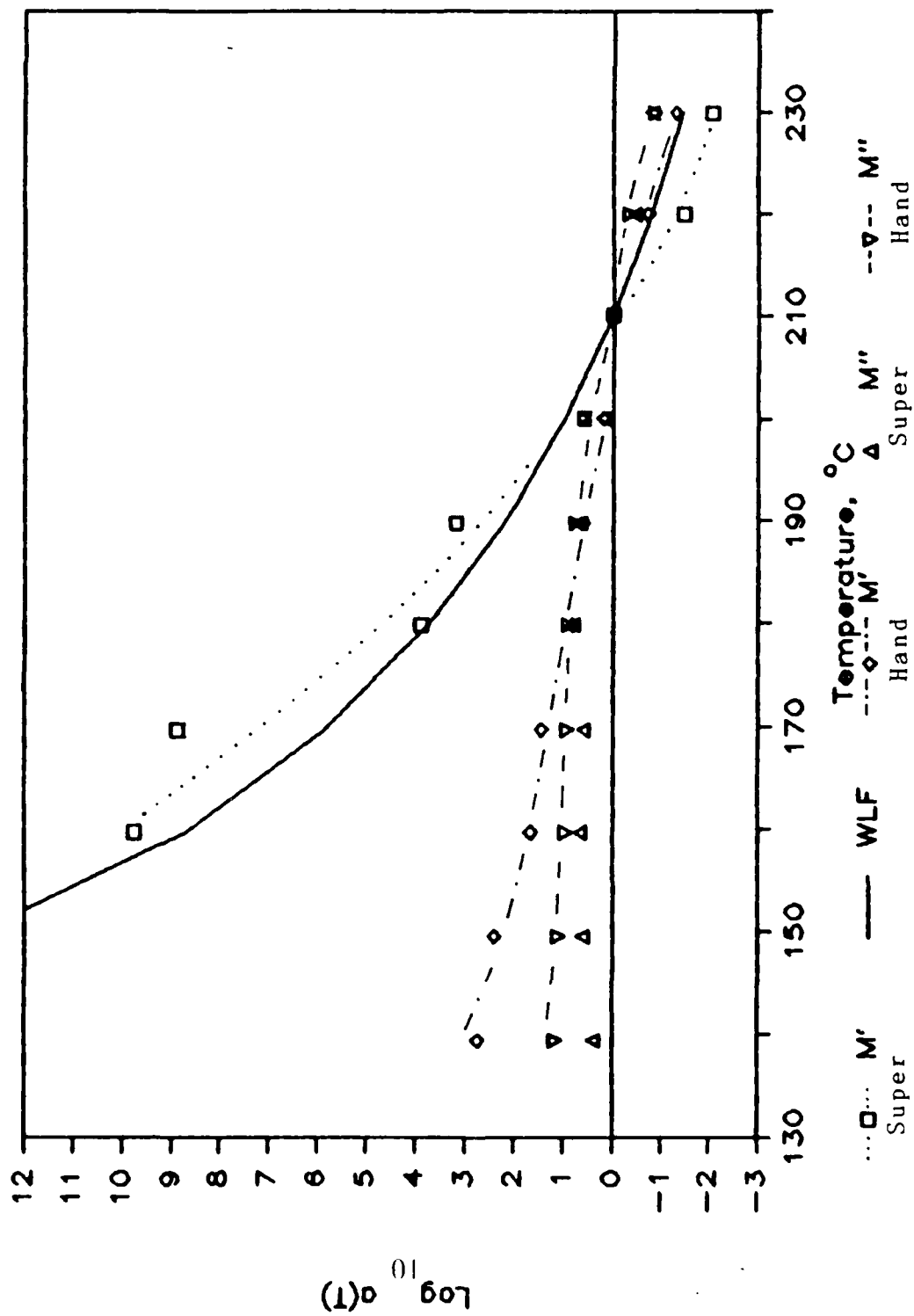


Fig. 11. Effect of Reduction Technique on 0° Specimen Shift Factors

Master Curves

Several master curves were drawn for the two specimen fiber orientations. In each case, the shift factors used are identified by computational method: by hand, or by eighth-order polynomial spline ("Super"). The moduli are weighted by the ratio of the reference temperature to actual temperature at which the data was obtained.

Figure 12 is the master curve for the 90° specimen generated by the Datalyzer "Super" routine for the storage modulus. Immediately noticeable are several gaps in the spectrum at the reduced frequencies above 100 GHz. These gaps in turn produce a huge overall bandwidth of the reduced frequency spectrum. This was caused by carrying out the frequency-temperature superposition for all temperatures, despite the assertion at the beginning of this chapter. The results clearly indicate the fallacy of extending superposition into the glassy region with noisy data.

Even in the applicable temperature regime, however, the large shift factor near the reference temperature leaves a gap in the master curve of the storage modulus just below 1 GHz. While the master curves at lower temperatures should not be displayed, this particular gap indicates that "Super" must still be supplemented with manual entries by the investigator.

The remaining portions of the master curves in Figure 12 resemble the complete curves presented in Figure 13, the

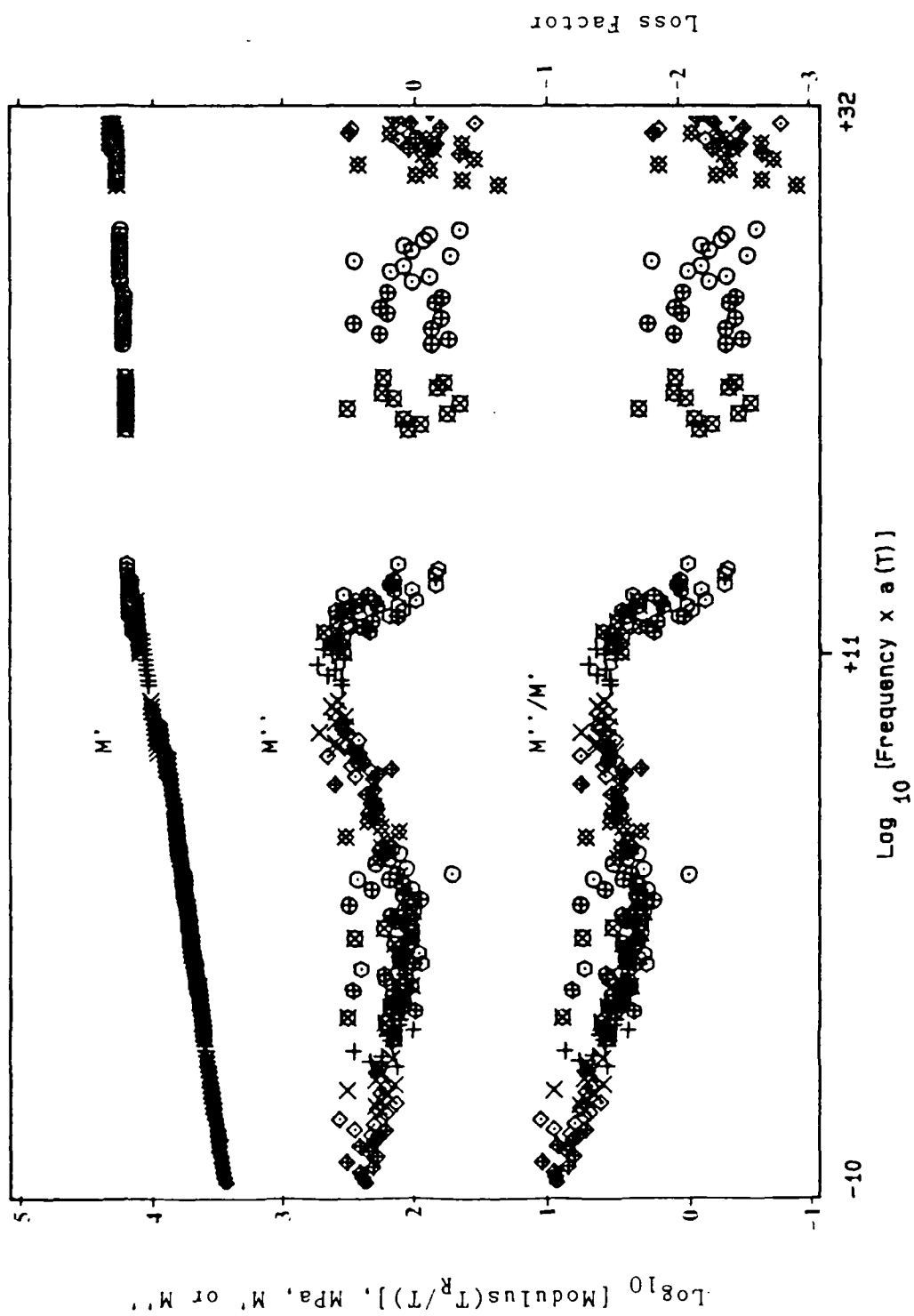


Fig. 12 Master Curves of 90° Beam From "Super" Shifts of Storage Modulus

master curves generated by hand for the storage modulus. In Figure 13, shifting was applied only near and above T_g . The storage modulus can be seen to decline at the lower frequencies in a manner similar to other highly crystalline polymers (11:42).

The loss modulus is very low in the region where the storage modulus changes slowly with frequency. The wide scatter at higher frequencies may be due to the presence of the fibers, but it also confirms the assertion that one can't apply frequency-temperature superposition to crystalline polymers in the glassy state (29:199). The broad transition region correlates with the observations at low strains of other polymers with an intermediate degree of crystallinity (29:219). The loss modulus increases with decreasing frequencies following a decline below the plateau-like transition region. This trend indicates the increasing viscoelastic nature of the composite above T_g .

The master curves for the 90° specimen developed by generating shifts relative to the loss moduli spectra are presented in Figures 14 and 15. The folding effect, or reversal of the master curve at low frequencies, from "Super" shifts is evident in Figure 14. This curve has little value.

In Figure 15, the loss modulus was used as a reference for hand shifting spectra only at temperatures above 120°C. Again, the broad, shallow peak in the loss modulus appears

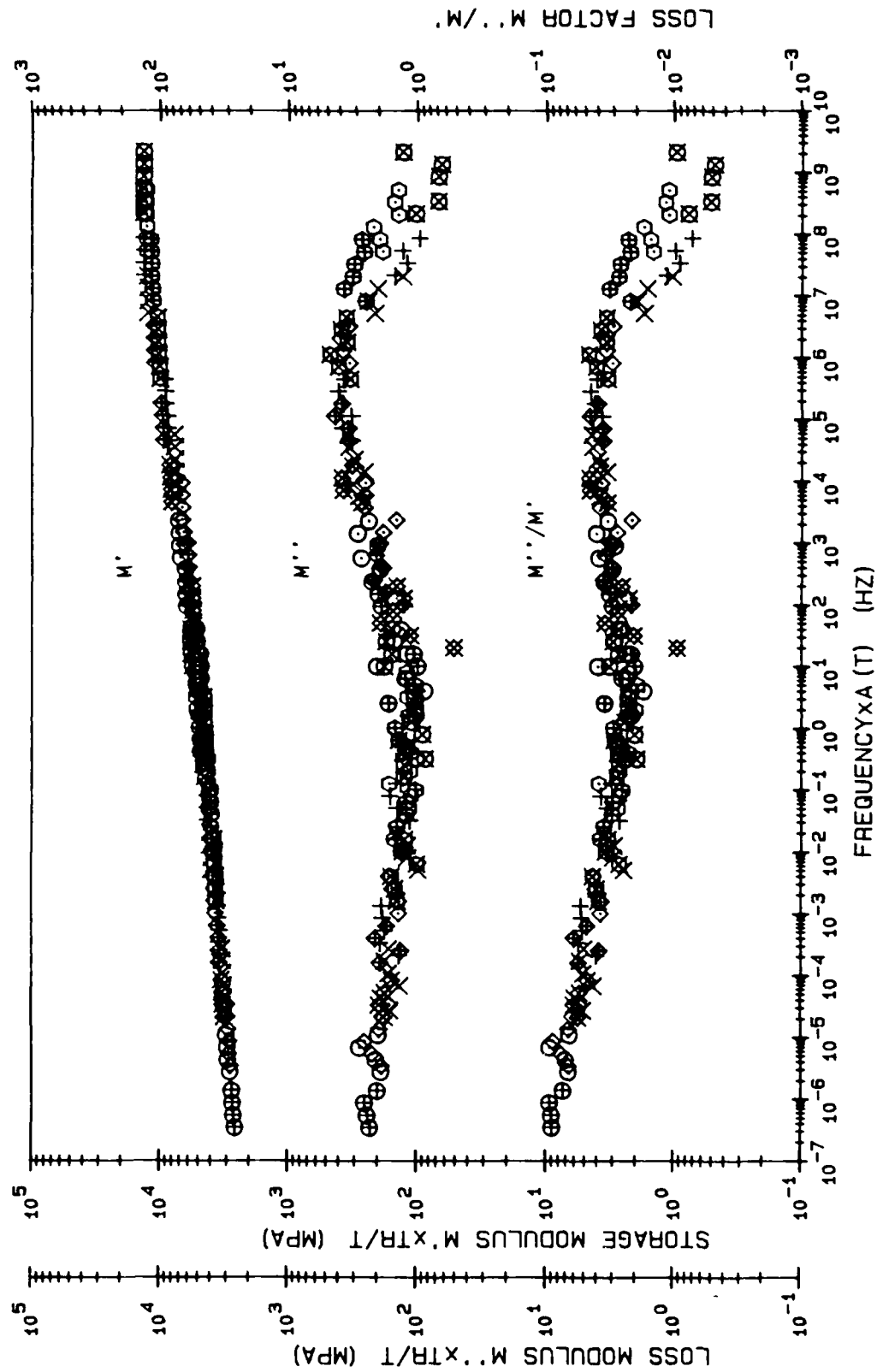


Fig. 13. Master Curves of 90° Beam From Hand Shifts of Storage Modulus

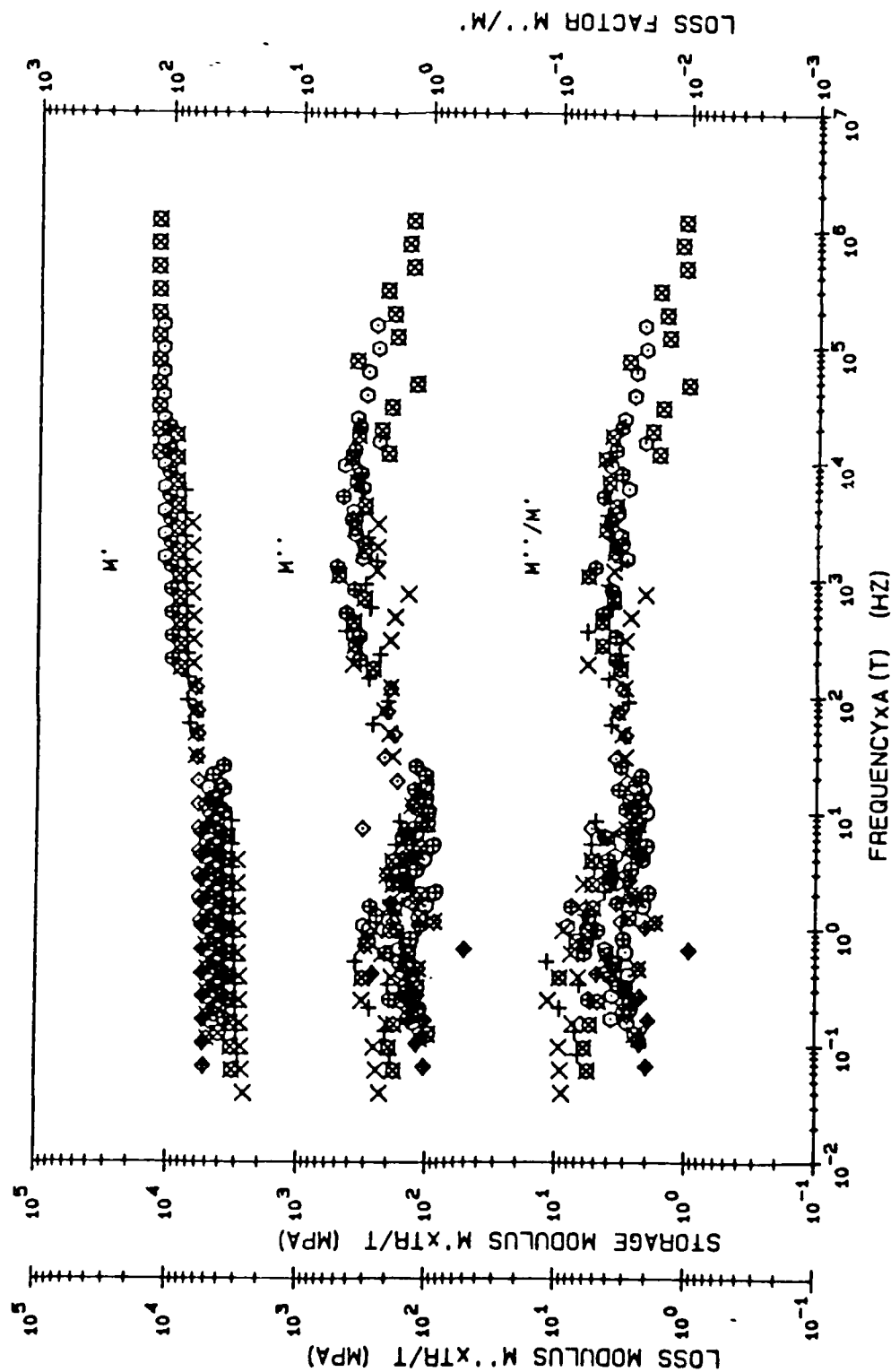


Fig. 14. Master Curves of 90° Beam From "Super" Shifts of Loss Modulus

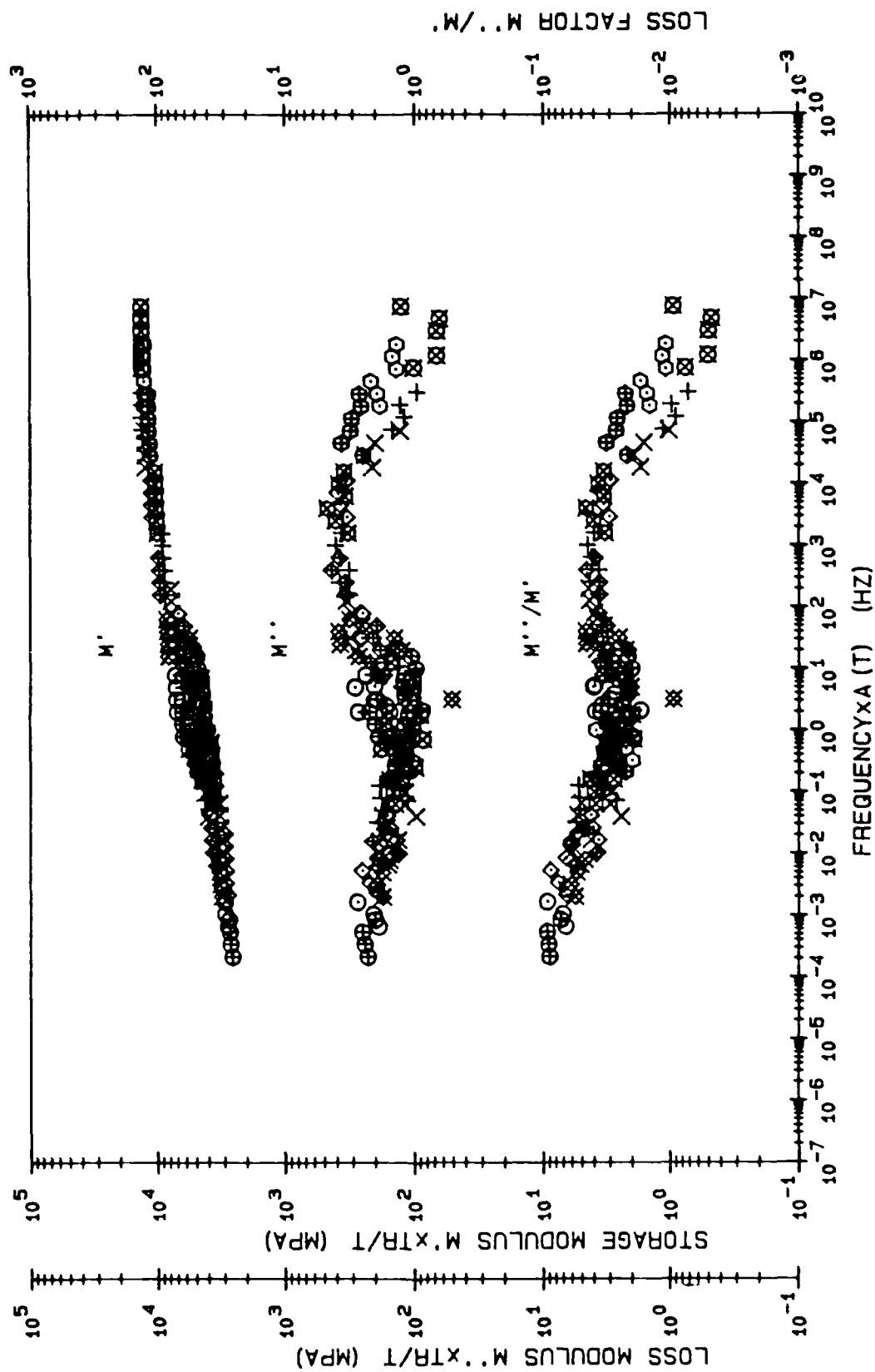


Fig. 15. Master Curve of 90° Beam From Hand Shifts of Loss Modulus

in the transition region. The loss modulus decreases with lower frequencies from this peak, and then increases with higher temperatures/lower frequencies.

The behavior of both moduli, and the loss factor, resembles the master curves constructed in Figure 13. Differences are seen mainly in the extension of the scale of the reduced frequency. The master curves generated from shift factors based on the storage modulus cover a wider range of frequencies. The master curves from the loss modulus shift factors indicate the range of values, or scatter, at a particular frequency.

The same approach as was just presented in detail for the 90° specimen produced master curves for the 0° specimen. Figures 16 and 17 display the results of shifting the storage modulus, with respect to a reference temperature of 210° C, by "Super" and by hand. As with the master curves of the 90° specimen, "Super" produces gaps of several decades and folds some spectra over others. There is little correlation of the resulting master curve to any trend. This demonstrates the inability of the Datalyzer to handle noisy or featureless data.

Shifting the data by hand, however, produces the broad, shallow peak in the out-of-phase response seen previously in the 90° sample. The range of values that the loss modulus and the loss factor take, in Figure 17, is one order of magnitude. The loss factor approaches small values near the

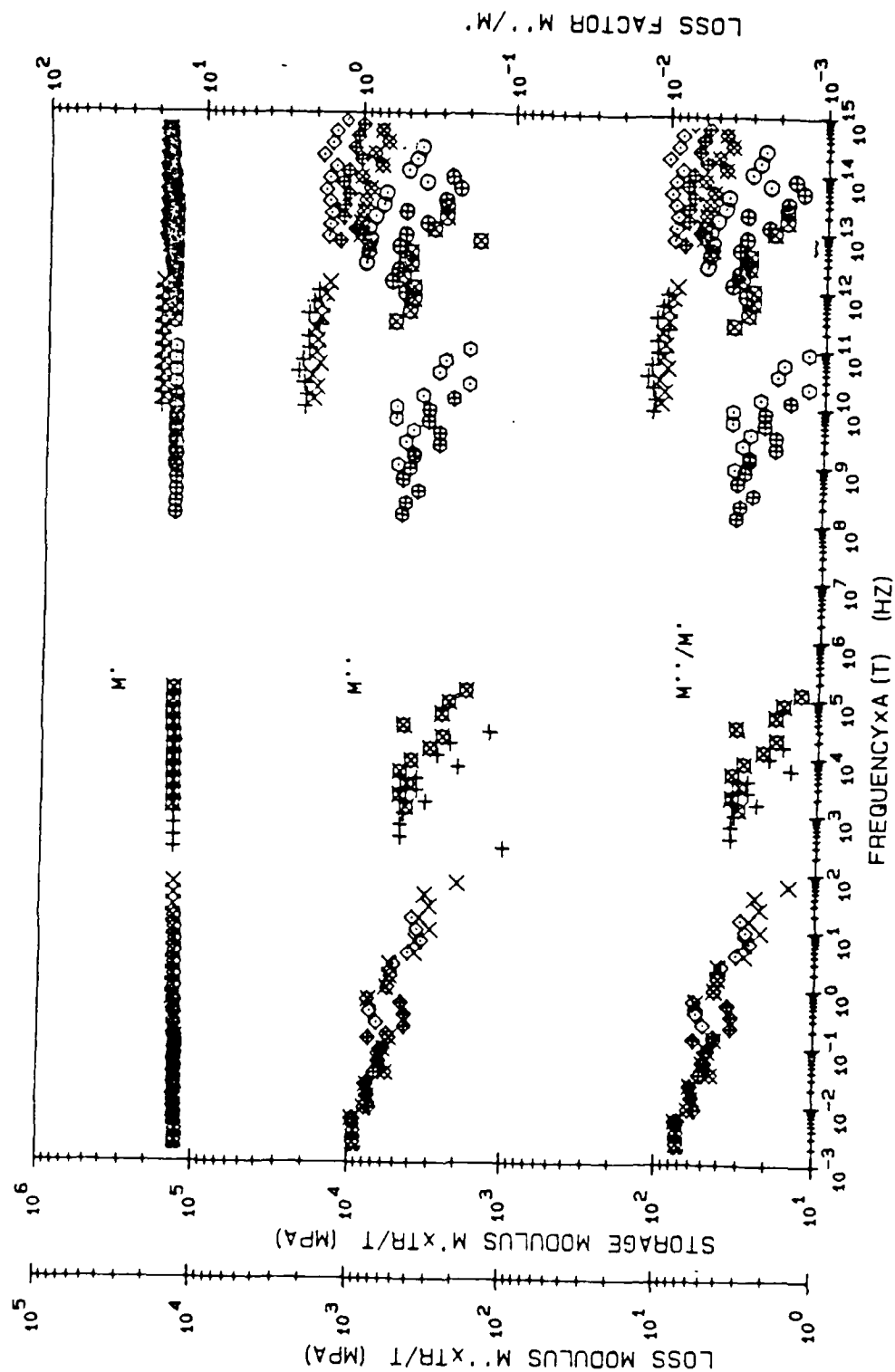


Fig. 16. Master Curves of 0° Beam From "Super" Shifts of Storage Modulus

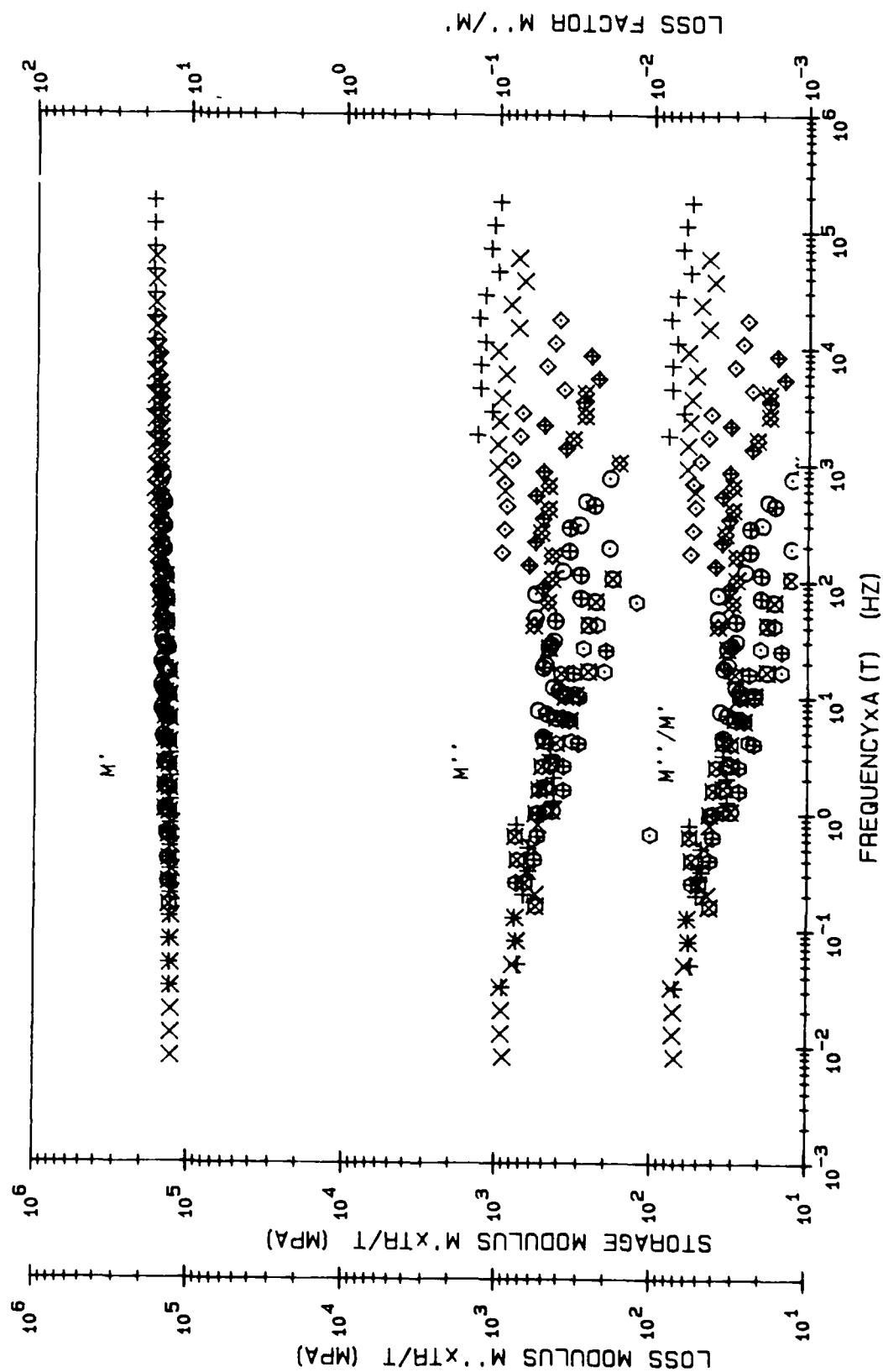


Fig. 17. Master Curves of 0° Beam From Hand Shifts of Storage Modulus

limit of the capability Dynastat to resolve mechanical response from noise. This behavior is expected for the fiber-dominated 0° specimen. The storage modulus declines only gradually through the transition region, and is nearly constant over a wide spectrum of low frequencies.

When the data is shifted with respect to the loss modulus, "Super" again folded the master curve over itself near the reference spectra between 1 Hz and 10Hz. Figure 18 shows this behavior, and is of little value.

The manual, or hand, shift factors produced the master curve presented in Figure 19. This curve shows the compression of the reduced frequency scale due to the difficulty of shifting noisy data by hand. It too is of little value.

Shear Deformation

Equation 15a predicts the flexural modulus with the contribution of shear deformation included. Table 3 incorporates the values for the shear modulus of APC-2 determined at 80°C and at 190°C by Tung and Dynes from Ref. 5. The experimentally determined values for the 0° specimen of the effective bending modulus, or complex modulus, at the same frequency as used in Ref. 5, are also listed. These values are then increased by the method described in the second chapter of this report. The results, tabulated in the far right column, approximate the parts of the effective flexural modulus due to bending alone for the given load. Shear deformation is seen to contribute to the total modulus by

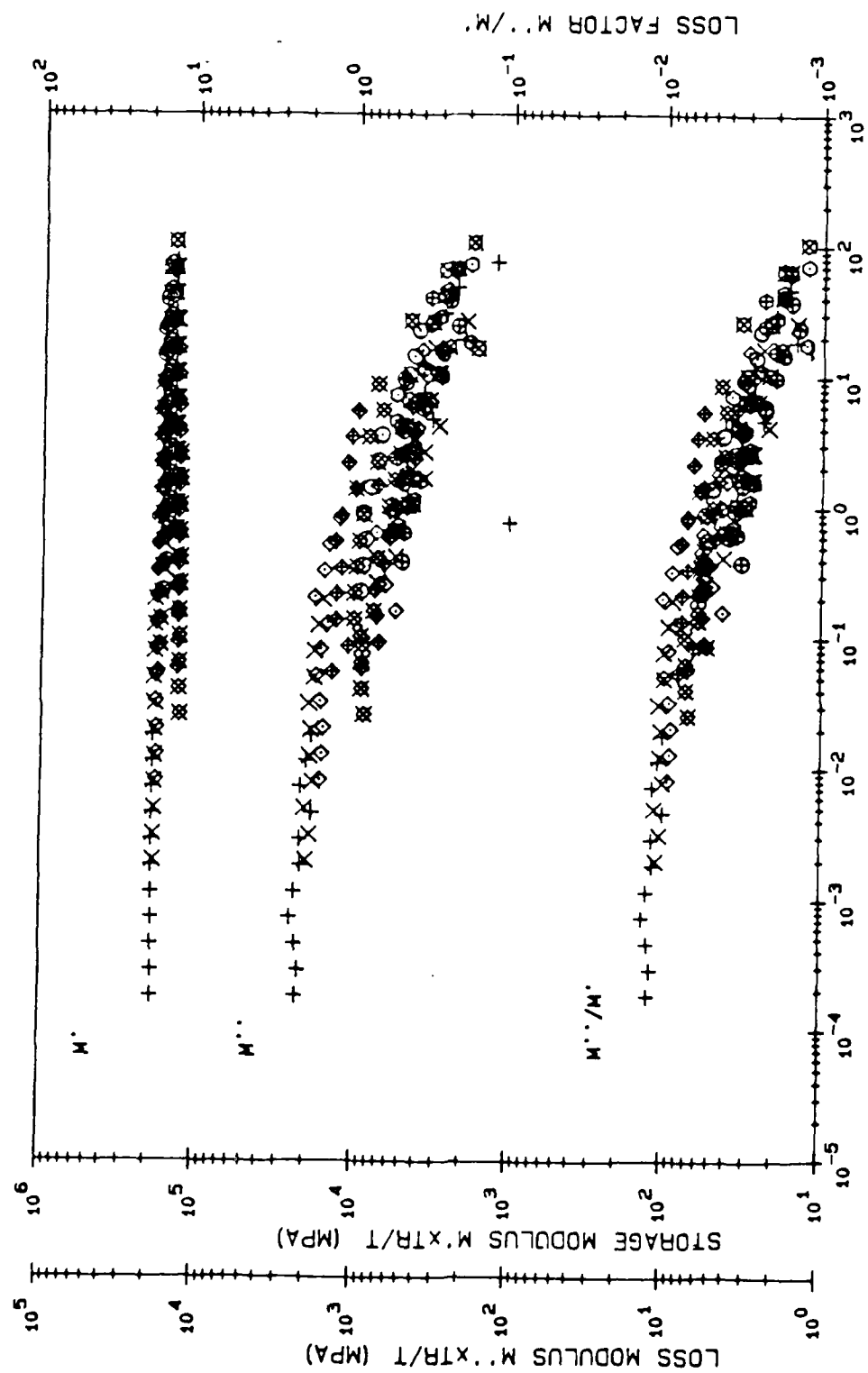


Fig. 18. Master Curves of 0° Beam From "Super" Shifts of Loss Modulus

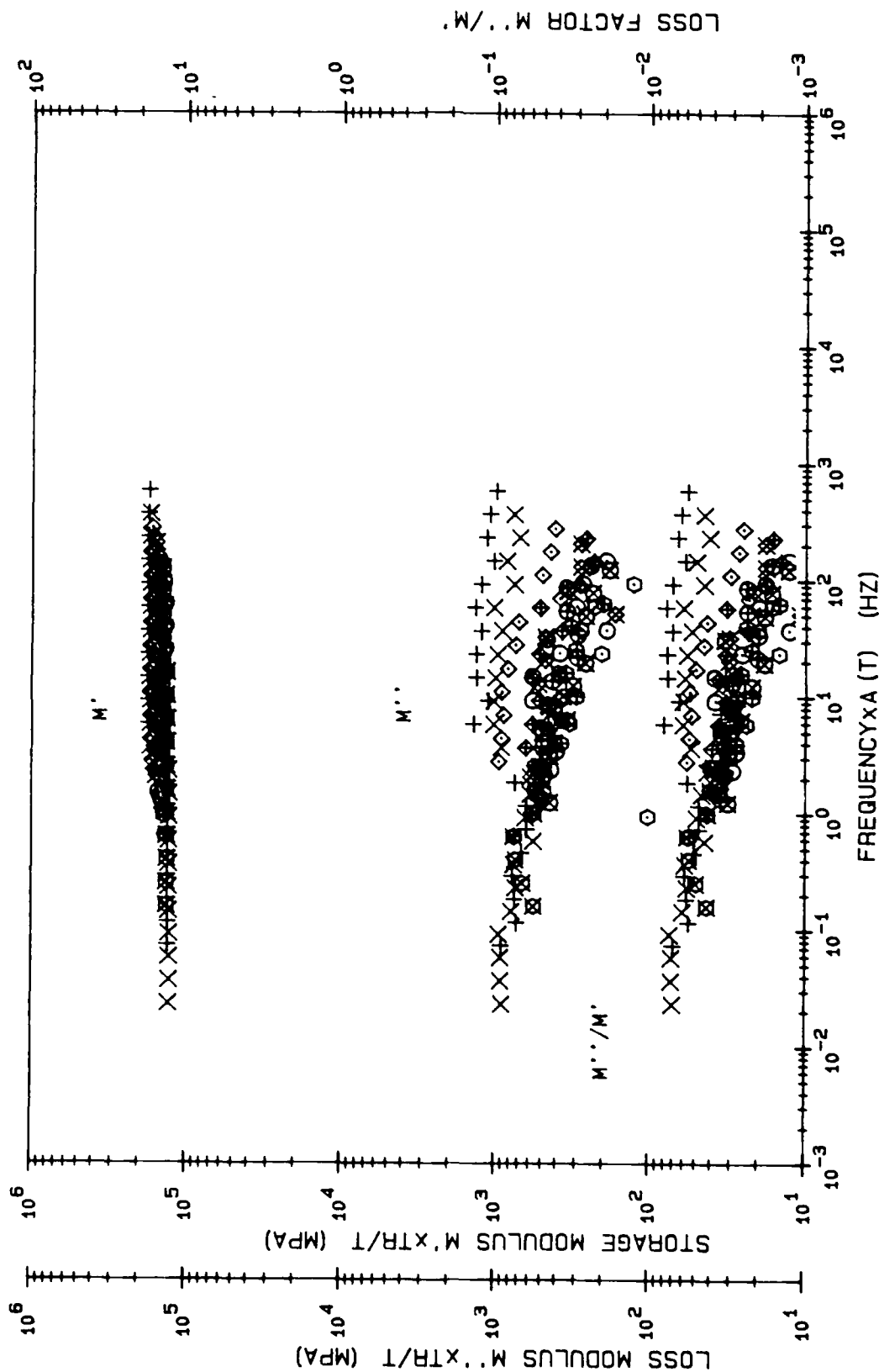


Fig. 19. Master Curves of 0° Beam From Hand Shifts of Loss Modulus

less than 8% at or below 190°C for these typical examples. Note Eqn. (15a) predicts an increase in \bar{E} with temperature. This isn't the general case. Rather, \bar{G} is so small around 190°C that Eqn. (15a) understates the contribution of shear deformation to the flexural modulus.

Table 3

Comparison of the Experimental Complex Flexural Modulus
With Shear Deformation Theory

Temperature (°C)	Maximum Center Span Load (N)	Experimental Flexural Modulus (GPa)	Shear Modulus (GPa)	Predicted Flexural Modulus (GPa)
80	7.57	136.8	4.9	139.6
190	7.38	133.3	2.28	143.5

Comparison to Rule of Mixtures Approach

The abbreviated frequency-temperature sweep conducted on the PEEK neat resin flexure sample obtained slightly ambiguous results. High temperature data is extremely suspect. The output of the load cell appeared as a clipped trace on the oscilloscope during some, but not all, of the cycles at each frequency at 210.8°C. The indenter rose off the sample at these points. This behavior was not repeated in later tests on composite samples. The difficulty in producing neat resin samples prevented a repeat in this test. It is not possible to say whether the cause of the

slipped waves was due to errors in technique, equipment failure, or friction between the specimen and the support or the indenter.

Confidence in the lower temperature data is better, though. Figure 20 shows the thermal dependence of the complex flexural moduli of the PEEK neat resin beam. Near and below T_g , there is little spread between data at each temperature. The overall behavior of the material resembles that of the matrix-dominated geometry (90° sample). The glassy region is evident, and a large peak occurs in the out-of-phase modulus near 160°C . The decrease in the loss modulus above T_g is less than the increase from the glassy region, as also exhibited by the composite.

The complex moduli corresponding to some of the data points plotted in Fig. 20 are repeated in Table 4. They are listed under the "Experiment" column for E_{11} (for the 0° sample) and E_{22} (for the 90° sample). Typical values are listed for one or two frequencies at each of the four temperatures at which neat resin flexural properties were established as just described.

The temperatures at which the neat resin data was obtained differ slightly from the actual temperatures at which the effective modulus data was obtained for the composite behavior. This difference has not been corrected, but is no more than 4.1°C for the two samples at any one temperature in Table 4. The 0° data at 13.9°C was obtained

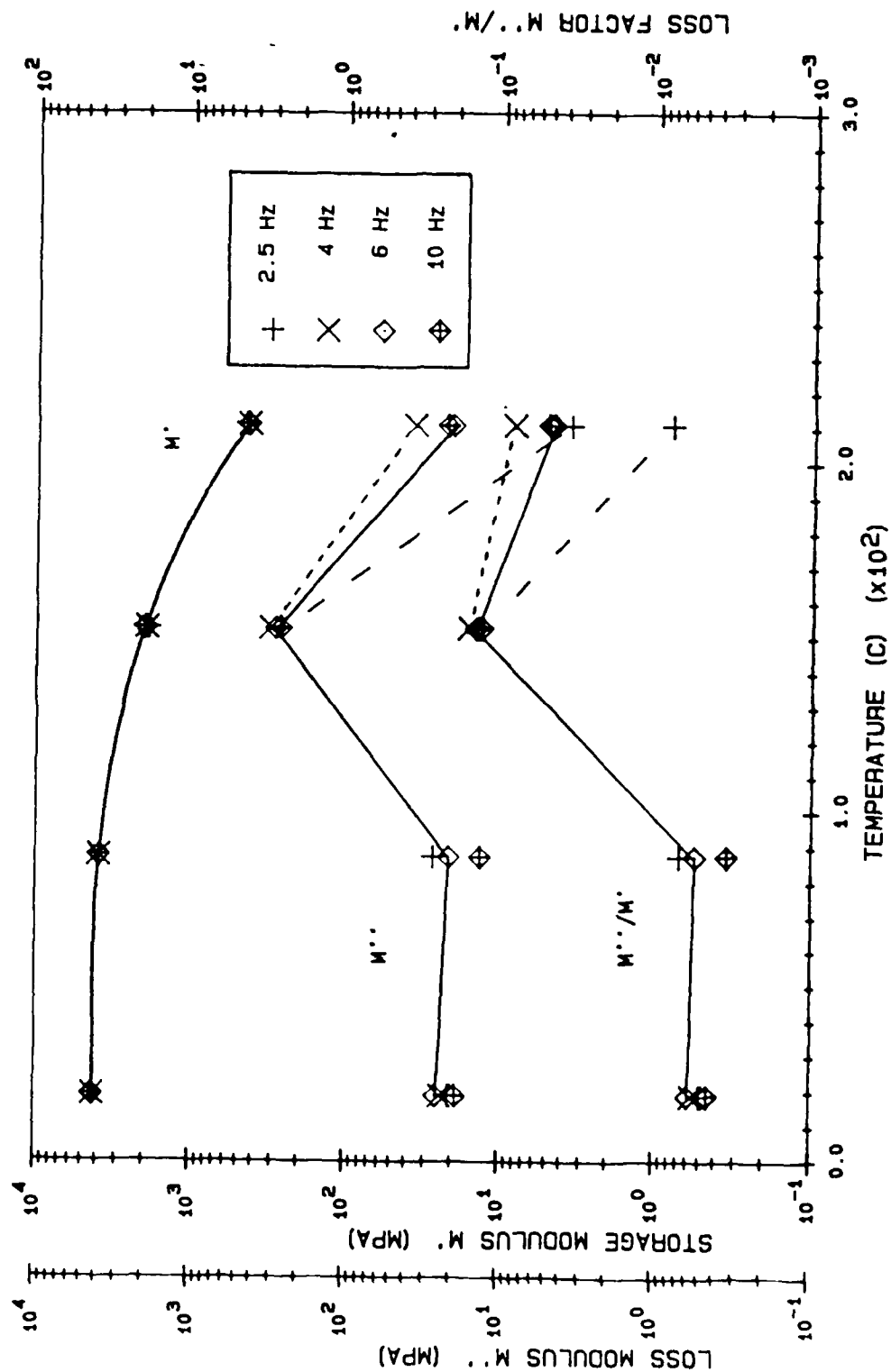


Fig. 20. Temperature Dependency of the Complex Flexural Moduli of PEEK

from a sample at room temperature from a different specimen than that used to obtain the results described earlier in this chapter.

Table 4
Comparison Between Experimental Flexural Moduli
And Values Predicted from the Rule of Mixtures

Temperature (°C)	Frequency (Hz)	E ₁₁		E ₂₂	
		Theory (GPa)	Experiment (GPa)	Theory (GPa)	Experiment (GPa)
(Fiber transverse modulus = 13.9 GPa)					
18.9	2.53	136.7	138.6	8.7	11.1
37.4	4.01	136.6	137.3	9.4	10.8
	6.36	136.6	136.9	9.4	10.8
152.5	6.36	136.0	135.0	5.0	7.0
	10.09	136.0	136.0	5.9	7.0
210.9	2.53	135.5	133.0	2.0	4.2
	10.09	135.5	133.2	1.9	4.9
(Fiber transverse modulus = 20.7 GPa)					
18.9	2.53	136.7	138.6	10.7	11.1
37.4	2.53	136.6	127.1	10.3	10.8
152.5	4.01	136.0	126.2	6.7	7.7
	10.09	136.0	136.0	6.9	7.0
210.9	2.53	135.5	133.0	2.1	4.2
	10.09	135.5	133.2	2.0	4.0

The composite effective flexural modulus can now be compared to predictions from Eqns. (15) and (17). Quasi-static values obtained from the dynamic flexure of specimens

were inserted into the static rule of mixtures developed by Halpin and Tsai.

One substitutes the volume fractions from Table 2 into Eqns. (16) through (18), and uses the neat resin data shown in Fig. 20. The lower and upper limits of the fiber transverse modulus (Reference 31) are both used in Eqn (17), yielding the range of quantities shown in Table 4 listed under the column heading "Theory".

The rule of mixtures predicts E_{11} in excellent agreement with experimental flexural moduli for the fiber and tested geometry. The range of values the fiber transverse modulus can take produces an acceptably narrow margin of error for temperatures near and below T_g .

It can not be asserted that the rule of mixtures fails at the highest temperature, as might be inferred from Table 4, because that is the point of questionable neat resin data. It is expected that higher quality data from the neat resin sample at 219.9°C would have yielded a higher matrix modulus, which in turn would have increased the theoretical value for E_{22} and thus decreased the discrepancies at that temperature.

Discrepancies between theory and experiment grow with increasing temperature, but have no particular trend with frequency at a given temperature. The fiber transverse modulus value of 10.7 GPa yields the best results. This is the upper limit of the range of values and may indicate that

a different value should be used for ξ than the Hewitt and deMolherbe relation would predict.

Discrepancies at all temperatures are also expected due to the different degrees of crystallinity of the PEEK neat resin sample and the matrix material of APC-2. This difference has been ignored until now, but appears to have only a small effect below and near T_g .

Shear Coupling Observations

A range of values for $\nu_{12}(\omega)$ from 0.16 to 0.22 for APC-2 does not appear unreasonable. The frequency and temperature dependence of the Poisson ratio of APC-2 were not experimentally confirmed in this research. The lower value was calculated by substituting minimum values for the matrix and fiber Poisson ratios into Egn. (12) (References 13 and 14). The lower and upper limits of the matrix Poisson ratio were taken to be 0.2 and 0.5, respectively. The lower and upper limits of the fiber Poisson ratio were taken to be 0.2 and 0.25, respectively. The maximum value calculated from Egn. (12) is less than that reported in Table 1, as the reported value was used for the maximum Poisson ratio for the composite.

A cursory examination of Egn. (7) reveals that the predicted difference between the actual tensile modulus and the experimentally determined effective longitudinal modulus will increase with an increase in the Poisson ratio of the material. Therefore, accepting 0.22 as a worst case value,

and for the length-to-width ratio of $L/b = 3.33$, the maximum corrections become factors of 1.035 for an isotropic beam and 1.91 for unidirectional APC-2.

Thus, by this method, the predicted value of the effective flexural modulus of APC-2 would differ from the tensile modulus by almost a factor of two. This occurs where ν_m is large, i.e., at higher temperatures. The discrepancy also shows the importance of properly sizing the flexure specimen, as noted previously (Reference 6). Mair concluded that the discrepancy decreased with increasing L/b ratios. The Dynastat test chamber was restricted in span, as mentioned in the previous chapter. Only by reducing the width would the effects of shear coupling become less noticeable, but this would have introduced the possibility of increased free edge effects.

Thus, shear coupling was not completely removed from the beam response. Experimental values otherwise show good agreement. One should observe, though, that Eqn. 7 should not be applied to angle-ply laminates, and, indeed, even corrections like Eqn. (7) may overestimate the flexural modulus by a factor of six (8:40).

V. Conclusion

Summary of Results

An analysis of three-point flexure for the viscoelastic characterization of a laminated composite of polyetheretherketone (PEEK) has been conducted based on an extension of laminated plate theory and the work of Whitney, Browning, and Mair. The results of a dynamic mechanical analysis of the thermoplastic matrix/graphite fiber composite APC-2 have been compared to the analytic model. Specimen geometry was selected to avoid any considerable warping due to shear deformation and biaxial response due to shear coupling.

Flexural data was obtained with a Dynastat viscoelastic dynamic and static analyzer over a two-decade frequency range and from roughly ambient temperatures to more than 230°C. Low strain levels produced a macroscopic linear stress behavior. Experimental flexural moduli at temperatures below 190°C, reduced from a model that neglects shear, match within 5% the predictions that include shear deformation. The T_g was measured to be between 150°C and 160°C for frequencies from 0.16 Hz (1 rad/sec) to 15.90 Hz (100 rad/sec).

Master curves have been created for the frequency-temperature behavior of two unidirectional geometries: one with the reinforcing fibers parallel with the longitudinal axis, the other with the fibers oriented transversely. The shift factors which generated the curves have been compared

by technique and judged for their effectiveness. The shift factors computed by the Dynastat for the storage modulus compare reasonably well with the WLF equation with standard constants. The Dynastat produced master curves similar to those created from shift factors determined by hand shifting the experimental data.

The effect of matrix viscoelasticity on the overall composite behavior was demonstrated in the master curves. The composite demonstrated nearly constant, fiber-dominated flexural rigidity even in the transverse geometry, but because of frequency- and temperature-dependent changes in the loss factor of one magnitude in order, the damping characteristics of the composite vary significantly. Broad, shallow peaks in the loss modulus and the loss factor in a transition zone correlate well with neat resin flexural behavior. After declining with lower frequencies from the transition zone, the out-of-phase components increased at extremely low frequencies in a manner indicating the viscoelastic effect increased with temperature above T_g . These trends were observed in both geometries at roughly the same frequencies and temperatures.

Neat resin response in flexure at a smaller number of temperatures and frequencies was obtained and incorporated in a rule of mixtures approach to predict composite behavior. Where high quality neat resin data was available, the predictions compared well with the experimental results.

Conclusions

The objectives of this research are repeated here.

Objective 1. Evaluate the flexural test and account for shear and Poisson effects. The viscoelastic behavior of APC-2 is predicted adequately by adapting elastic static plate theory to the dynamic flexure of unidirectional laminates. The degree of APC-2 anisotropy is not significant at the load levels within this research. Shear deformation, Poisson effects, and shear coupling do not contribute significantly to the effective flexural modulus determined by the three point bend test if one properly sizes the specimen geometry and uses small deformations as in this research.

Objective 2. Characterize the frequency and temperature dependency of APC-2 in dynamic flexure. The complex flexural modulus of APC-2 reflects a strong fiber dominance which suppresses the out-of-phase component. Master curves of unidirectional laminates are extremely difficult to obtain. Best results are obtained for the matrix dominated flexure geometry (90° sample). When based on the behavior of the storage modulus, the master curves do exhibit the expected viscoelastic nature of the thermoplastic matrix.

Master curves should not be generated from the behavior of the loss modulus of composite materials. The loss modulus data must be of high quality and exhibit marked frequency and temperature characteristics.

The presence of fibers in the matrix dominated orientation slightly increases the glass transition temperature of APC-2 from the T_g of PEEK. Otherwise, the effective flexural modulus of this thermoplastic composite can be predicted, from a rule of mixtures approach, if quasi-static behavior is assumed, the effects of crystallinity are considered, and the unidirectional fibers are oriented transverse to the neutral axis of the beam.

The presence of fibers alters the temperature dependency of the out-of-phase component of the complex flexure modulus for the composite with fibers aligned parallel with the neutral axis. The viscoelastic effect is unexpectedly high in the glassy region. This behavior is currently unexplained, and merits further research.

Objective 3. Compare the frequency-temperature shift factors obtained in three ways: analytically, using the WLF equation; experimentally, using the Dynastat curve-fitting algorithm; and manually, using hand-shifted values from experimental results. As mentioned previously, the highest quality master curves were produced by the Dynastat by shifting the storage modulus spectra for the 90° sample. These shift factors most closely resemble the behavior of a thermorheologically simple solid that the WLF equation models. The difference between the Dynastat shift factors and those obtained manually can be expected to decrease with operator experience with the manual technique. However, the

Dynastat can provide reliable and good resolution data. The automatic curve-fitting capability is useful as a first step in calculating frequency-temperature superpositions. Its utility in reducing the time required to generate shift factors, and plot the subsequent master curves, is evident. The results, however, must be obtained from test conditions known to produce linear behavior with a high signal to noise ratio.

Recommendations

The analysis employed in this study appears valid for unidirectional, anisotropic, laminated composite materials with high flexural rigidities. However, future studies should employ some experimental modifications:

1. Flexure tests should cover a wider range of temperatures than used in this research. The cryogenic and near-melt temperature regions were not included here, and much useful design information can be obtained from their inclusion into a test plan.

2. Apart from an increase in the signal to noise ratio that the experimental method produces, frequency-temperature shifting requires data with better features. Combinations of the following steps may improve the capability of the Dynastat and the three point flexure test to obtain visco-elastic characteristics of composite laminates. The temperature increment should be decreased near T_g , or the number of discrete frequencies used at each temperature should be

increased. This should yield polynomial curve fits of the modulus spectra that will be less susceptible to noise and slope changes at the ends of the splines.

3. The Materials Laboratory should investigate the feasibility of using four point flexure in future viscoelastic characterizations. This loading subjects the center span of the flexure specimen to a constant bending moment and more accurately resembles a state of pure bending. The three dimensional state of stress at the supports and indentors will of course still exist, but it may not introduce as many complications to the analysis.

4. Tensile tests of APC-2 coupons may better define the frequency-temperature dependence of the Poisson ratio. Shear coupling effects of other laminates to be tested on the Dynastat in the future may be better controlled by this knowledge.

5. The Materials Laboratory should investigate the feasibility of using test chamber supports with longer spans for the Dynastat. This would additionally minimize shear coupling and free edge effects.

6. Finally, the test technique to be used with the Dynastat must improve the signal to noise ratio observed in this research. Observations over 15 cycles should be used with stiff composites, while a smaller number of cycles may still be adequate with homogeneous isotropic viscoelastic materials. If necessary, higher deformations should be used

as a last resort to produce higher load cell signals. It will still be necessary to ensure all deflections produce linear behavior.

Bibliography

1. Bishop, Sarah M. "The Mechanical Performance and Impact Behaviour of Carbon-fibre Reinforced PEEK," Composite Structures, 3:295 (1985).
2. Stcher, Eric J. et al. "Characterization and Exposure of Polyetheretherketone (PEEK) to Fluid Environments," Polymer, 25:1845 (December 1984).
3. Jones, D.P. et al. "Mechanical Properties of Poly (ether-ether-ketone) for Engineering Applications," Polymer, 26: 1385 (August 1985).
4. Gebe, Peggy et al. "Effect of Thermal History on Mechanical Properties of Polyetheretherketone below its Glass Transition Temperature," Journal of Applied Polymer Science, 32: 487 (1987).
5. Tung, C.M. and P.J. Dynes. "Morphological Characterization of Polyetheretherketone Carbon Fiber Composites," Journal of Applied Polymer Science, 33: 487 (1987).
6. Whitney, J.M. et al. "Analysis of the Flexure Test for Laminated Composite Materials," Composite Materials: Testing and Design (3rd Conference), ASTM STP 546. Baltimore: American Society for Testing and Materials, 1974.
7. "Standard Test Methods for Flexural Properties of Thermoset and Reinforced Plastics and Electrical Insulating Materials (Metric)," Annual Book of ASTM Standards, 98.01: 410 (September 1984).
8. Mair, Capt Alexander. Analysis of Beam Bending Experiments on Off-Axis Laminated Composites. MS Thesis, AFIT/GAM/MC/72-3. School of Engineering, Air Force Institute of Technology (AU), Wright Patterson AFB OH, December 1972.
9. Sims, D.E. and J.C. Halpin. "Methods for Determining Elastic and Viscoelastic Response of Composite Materials," Composite Materials: Testing and Design (3rd Conference), ASTM STP 546. Baltimore: American Society for Testing and Materials, 1974.
10. Jones, Robert M. Mechanics of Composite Materials. New York: Hemisphere Publishing Co., 1975.

11. Ferry, J.D. Viscoelastic Properties of Polymers. New York: John Wiley & Sons, Inc., 1980.
12. Johnston, Norman J. and Paul M. Hergenrother. "High Performance Thermoplastics: A Review of Host Resin and Composite Properties," Advanced Materials Technology 197 (32nd International CAMPE Symposium), 32:1420 (1987).
13. Anderson, David, Non-Metallics Division, Structural Materials Branch. Personal interview. AFWAL, Wright-Patterson AFB OH, 1 July through 26 October 1987.
14. Victrix Resins. Product catalog ME 2427. ICI Americas Inc., Wilmington, DE, undated.
15. Sternstein, S.S. "Transient and Dynamic Characterization of Viscoelastic Solids," Polymer Characterization. Washington, D.C., American Chemical Society, 1985.
16. Synstat Operating Manual. Imasco, Inc., Hingham, MA, August 1988.
17. Whitney, J.M. "Elastic Moduli of Unidirectional Composites with Anisotropic Filaments," Journal of Composite Materials, 1: 122 (1967).
18. Synatherm Operating Manual. Imasco, Inc., Hingham, MA, August 1988.
19. The Dynalizer and Sealer. Product Bulletin DC 4-88. Imasco, Inc., Hingham, MA, undated.
20. Van der Ey, G. A. "Equations of the Continuum Theory of Composite Materials," Fibrous Composites (Kompozitsionnye materialy voloknistogo stroyeniya), edited by I. N. Frantsevich and D. M. Karpinos, English translation by Keter Press, Jerusalem, 1973.
21. Bert, C. W. "Composite Materials: A Survey of the Damping Capacity of Fiber Reinforced Composites," Damping Applications for Vibration Control, edited by Peter J. Torvik. New York: American Society of Mechanical Engineers, 1980.
22. Ashton, J. E. and J. M. Whitney. Theory of Laminated Plates. Stamford, CT: Technomic Publishing Co., Inc., 1970.
23. Schultz, A. B. and C. W. Tzou. "Dynamic Moduli and Damping Ratios in Fiber Reinforced Composites," Journal of Composite Materials, 2: 260 (Nov. 1, 1968).

24. Lee, Charles Y.-C., et al. Dynamic Mechanical Measurement of Polyphenylsulfone (Radel). Interim Technical Report AFML TR-79-4062, AFWAL, Wright Patterson AFB OH, June 1979.
25. Tsai, Stephen W. and H. Thomas Mahan. Introduction to Composite Materials. Westport, CT: Technomic Publishing Co., Inc., 1980.
26. Srinivasan, K., et al. "Mechanical and Optical Characterization of Thermoplastic Matrix Composites," ACS Preprints, 26: No. 1, 279 (1985).
27. Whitney, J. M. Testing and Characterization of Composite Materials. AFML TR 71 124, AFWAL. Wright Patterson AFB OH, 1971.
28. Williams, M. L. "Structural Analysis of Viscoelastic Materials," AIAA Journal, 2: 725 (Vol. 5, May 1967).
29. Dillmeyer, Fred W. Textbook of Polymer Science. New York: John Wiley & Sons, Inc., 1971.
30. Chames, Irving H. and Clive L. Dym. Energy and Finite Element Methods in Structural Mechanics. Washington, D. C.: Hemisphere Publishing Corp., 1985.
31. Whitney, James, Non-Metallifer Division, Structural Materials Branch. Personal interview. AFWAL, Wright Patterson AFB OH, 20 October 1987.

VITA

Captain Richard P. Lockwood was born on 24 November 1957 in Warwick, Rhode Island. He graduated from high school in Lexington Park, Maryland in 1976 and attended the University of Maryland, College Park, from which he received the degree of Bachelor of Science in Aerospace Engineering in December 1980. Upon graduation, he received a commission in the USAF through the ROTC program. He completed undergraduate navigator training. He received his wings in November 1981, and completed Electronic Warfare Officer Training in May 1982. He then served as an engineering project manager in the 475th and 4484th Test Squadrons, Tyndall AFB, Florida, until entering the School of Engineering, Air Force Institute of Technology, in June 1986.

Permanent address: 103 Rison Road

Lexington Park, Maryland 20653

P 11045

REPORT DOCUMENTATION PAGE

Form Approved
OMB No. 0704-0188

1. REPORT SECURITY CLASSIFICATION UNCLASSIFIED		1b. RESTRICTIVE MARKINGS		
2a. SECURITY CLASSIFICATION AUTHORITY		3. DISTRIBUTION / AVAILABILITY OF REPORT Approved for public release; distribution unlimited.		
2b. DECLASSIFICATION / DOWNGRADING SCHEDULE				
4. PERFORMING ORGANIZATION REPORT NUMBER(S) AFIT/GAE-AA/87D-10		5. MONITORING ORGANIZATION REPORT NUMBER(S)		
6a. NAME OF PERFORMING ORGANIZATION School of Engineering	6b. OFFICE SYMBOL (If applicable) AFIT/ENY	7a. NAME OF MONITORING ORGANIZATION		
6c. ADDRESS (City, State, and ZIP Code) Air Force Institute of Technology (AU) Wright-Patterson AFB, OH 45433-6583		7b. ADDRESS (City, State, and ZIP Code)		
8a. NAME OF FUNDING SPONSORING ORGANIZATION Non-Metallics Division, Structural Materials Branch	8b. OFFICE SYMBOL (If applicable) AFWAL/MLBC	9. PROCUREMENT INSTRUMENT IDENTIFICATION NUMBER		
8c. ADDRESS (City, State and ZIP Code) Air Force Wright Aeronautical Laboratories Wright-Patterson AFB, OH 45433-6533		10. SOURCE OF FUNDING NUMBERS		
		PROGRAM ELEMENT NO	PROJECT NO	
		TASK NO	WORK UNIT ACCESSION NO	
11. TITLE (Include Security Classification) VISCOELASTIC BEHAVIOR OF A POLYETHERETHERKETONE (PEEK) COMPOSITE				
12. PERSONAL AUTHOR(S) Richard P. Lockwood, B.S., Capt, USAF				
13a. TYPE OF REPORT MS Thesis	13b. TIME COVERED FROM _____ TO _____	14. DATE OF REPORT (Year, Month, Day) 1987, December	15. PAGE COUNT 91	
16. SUPPLEMENTARY NOTATION				
17. COSAT CODES		18. SUBJECT TERMS (Continue on reverse if necessary and identify by block number) Viscoelasticity, Thermoviscoelasticity, Thermoplastic resins, Reinforced plastics, Fiber orientation, Mechanical properties, Fiber composites.		
FIELD	GROUP			SUB-GROUP
11	09			
19. ABSTRACT (Continue on reverse if necessary and identify by block number) Thesis Chairman: Paul D. Copp, Major, USAF Assistant Professor of Mechanics				
20. DISTRIBUTION / AVAILABILITY OF ABSTRACT <input checked="" type="checkbox"/> UNCLASSIFIED / UNLIMITED <input type="checkbox"/> SAME AS RPT <input type="checkbox"/> DTIC USERS		21. ABSTRACT SECURITY CLASSIFICATION UNCLASSIFIED		
22a. NAME OF RESPONSIBLE INDIVIDUAL Paul D. Copp, Major, USAF		22b. TELEPHONE (Include Area Code) (513) 255-2362	22c. OFFICE SYMBOL AFIT-ENY	

Approved for
Lynd E. V. C. E.
Dean for Research
Air Force Institute of Technology
Wright-Patterson AFB, OH 45433-6533
31 Oct 87
Deployment

Abstract

The thermoplastic polyetheretherketone (PEEK) is being considered for structural applications in the Advanced Tactical Fighter. Previous efforts characterizing PEEK mechanical properties are reviewed. A study developing the viscoelastic frequency-temperature response to three point flexure of neat resin and PEEK/graphite fiber composites is detailed. The behavior of unidirectional laminates is compared to predictions from elastic plate theory, which also combines micro- and macromechanical approaches to predict transverse and longitudinal complex moduli. The experimental frequency-temperature shift factors, obtained under low strain in a Dynastat dynamic viscoelastic analyzer, are compared to shift factors predicted from the Williams-Landel-Ferry equation. Determining composite behavior from knowledge of matrix and fiber behavior is still applicable. The capability of the Dynastat to perform viscoelastic characterizations of stiff, unidirectional composites, based on comparisons of the various shift factors, is reduced due to the presence of the reinforcing fibers. Recommendations for future test and evaluations, including increasing the dynamic signal-to-noise ratio, are described.

EW D
DATE
FILMED
3-1988
DTIC